PB-223 628

DEVELOPMENT OF IN SITU PROTOTYPE DIODE LASER SYSTEM TO MONITOR SO2 ACROSS THE STACK

MASSACHUSETTS INSTITUTE OF TECHNOLOGY

PREPARED FOR
ENVIRONMENTAL PROTECTION AGENCY

MAY 1973

DISTRIBUTED BY:

NTIS
National Technical Information Service
U. S. DEPARTMENT OF COMMERCE

BIBLIOGRAPHIC DATA SHEET	1. Report No. EPA-R2-73-218	2	3. Recipient's Accession No. PB-223 628
4. Title and Subtitle Development of In Situ Prototype Diode Laser System to Monitor SO_2 Across the Stack			5. Report Date May 1973 6.
7. Author(s) E. David Hinkley			8. Performing Organization Rept. No.
9. Performing Organization Name and Address Lincoln Laboratory Massachusetts Institute of Technology P.O. Box 73 Lexington, Massachusetts 02173			10. Project/Task/Work Unit No. 11. Contract/Grant No. 68-02-0569
12. Sponsoring Organization Name and Address Environmental Protection Agency Division of Chemistry and Physics Research Triangle Park, N.C. 27711			13. Type of Report & Period Covered Final, 11/71-3/73 14.
15. Supplementary Notes			

16. Abstracts

This report describes the development and testing of a semiconductor diode laser system to monitor sulfur dioxide by differential absorption of infrared radiation. Laser material was prepared and diodes fabricated which would operate in a temperature-independent region of SO_2 absorption. Data concerning sensitivity and interferences from aerosols and other gases were recorded in the laboratory. Field tests were then performed at an operating coal-burning power generating station, with the results compared with SO_2 measurements taken with a conventional chemical monitor.

17. Key Words and Document Analysis. 17a. Descriptors

tunable infrared laser
differential absorption
infrared detection
in situ monitoring

17b. Identifiers/Open-Ended Terms

Reproduced by
NATIONAL TECHNICAL INFORMATION SERVICE
US Department of Commerce
Springfield, VA. 22151

17c. COSATI Field/Group

18. Availability Statement	19. Security Class (This Report)	21. No. of Pages
Release unlimited	UNCLASSIFIED	
	20. Security Class (This Page) UNCLASSIFIED	22. Price

EPA-R2-73-218

Development of In-Situ Prototype Diode Laser System to Monitor SO_2 Across the Stack

by

E. D. Hinkley

Massachusetts Institute of Technology
Lincoln Laboratory
Lexington, Massachusetts

Contract No. 68-02-0569
Program Element No. 1A1010

EPA Project Officer: John S. Nader

Chemistry and Physics Laboratory
National Environmental Research Center
Research Triangle Park, North Carolina 27711

Prepared for

OFFICE OF RESEARCH AND MONITORING
U. S. ENVIRONMENTAL PROTECTION AGENCY
WASHINGTON, D.C. 20460

May 1973

This report has been reviewed by the Environmental Protection Agency and approved for publication. Approval does not signify that the contents necessarily reflect the views and policies of the Agency, nor does mention of trade names or commercial products constitute endorsement or recommendation for use.

CONTENTS

Section		Page
1	INTRODUCTION AND SUMMARY	1
	1.1 Background	1
	1.2 Present Effort	2
2	SYSTEM DESIGN	3
	2.1 Sulfur Dioxide Absorption Spectrum	3
	2.2 Infrared Detector and Filter Assembly	5
	2.3 System Operation	7
3	DIODE LASER DEVELOPMENT	9
	3.1 Crystal Growth	9
	3.2 Electrical Contacts	10
	3.3 Preparation of Laser Cavity	10
	3.4 Summary	10
4	CHARACTERISTICS OF DIODE LASERS USED IN MONITORING SYSTEM	11
	4.1 Possible Monitoring Techniques	11
	4.2 Properties of Diode Lasers Used in System	12
5	LABORATORY TESTS	17
	5.1 Sensitivity	17
	5.2 Linearity	19
	5.3 Interferences Due to Smoke, Water Vapor, and Steam	19
	5.4 Interferences Due to Other Gases: NH_3, C_2H_4	23
6	FIELD TESTS	24
	6.1 Helium-Neon Laser Transmission Across an Oil-Burning Stack	24
	6.2 In-Stack Measurements (Oil/Natural Gas) Using Diode Laser	27
	6.3 On-Line SO_2 and Transmission Measurements at a Coal-Burning Power Plant	31
7	RECOMMENDATIONS FOR FUTURE STUDIES	33
	7.1 Temperature Dependence	33
	7.2 Interferences from Other Gases	33
	7.3 Laser Tuning and Directionality	34
Acknowledgments		35
References		35
Appendix A:	Operating and Circuit Details	37
Appendix B:	Tunable Infrared Lasers and Their Applications to Air Pollution Measurements	54

The work reported here was performed by:

E. D. Hinkley

J. O. Sample

L. B. McCullough

A. R. Calawa*

T. C. Harman*

J. P. McVittie*

J. N. Walpole*

L. J. Belanger*

A. E. Paladino*

J. H. Boghos*

S. Duda*

J. N. McMillan*

* Denotes part time.

DEVELOPMENT OF IN SITU PROTOTYPE DIODE LASER SYSTEM TO MONITOR SO_2 ACROSS THE STACK

1. INTRODUCTION AND SUMMARY

Eventual application of tunable lasers in air pollution monitoring has been significantly advanced by recent developments both in laser technology[1] and in the realization that certain remote sensing techniques can become more sensitive and specific when tunable lasers are used.[2] Semiconductor diode lasers have been in the forefront of these advances because of their ability to match strong infrared spectral lines of the known pollutant gases, their simplicity of design and operation, and prospects for low ultimate cost.

This program is an outgrowth of an earlier experimental effort[3] which investigated the potential of tunable diode lasers for point sampling, in situ source monitoring, ambient air monitoring, and single-ended, passive heterodyne detection. In this report are described the development and operation of an experimental diode laser system for the monitoring of sulfur dioxide (SO_2) in power plants by across-the-stack in situ measurements. Data related to the particulate loading are recording simultaneously. The infrared laser and detector are cooled with liquid helium for this research prototype. Analog readout of the SO_2 concentration and percent transmission of laser energy across the stack is recorded on a strip chart; digital readout of time, SO_2 ppm, and percent transmission is performed by a digital clock, panel meter, and printer.

1.1 Background

Semiconductor diode lasers can be tailored to emit in desired wavelength regions by control of the energy gap – a feature made possible by the development of ternary semiconductor compounds of adjustable chemical composition.[4] The different materials from which semiconductor lasers have been made are shown in Fig. 1. Complete coverage of the region between 0.63 and 34 μm is now possible. The dashed lines indicate possible future extension of the present limits (solid lines). Most of the tunable diode laser work has been performed with the lead chalcogenides $Pb_{1-x}Sn_xTe$ (between 6.5 and 34 μm), $PbS_{1-x}Se_x$ (between 4.0 and 8.5 μm), and $Pb_{1-x}Cd_xS$

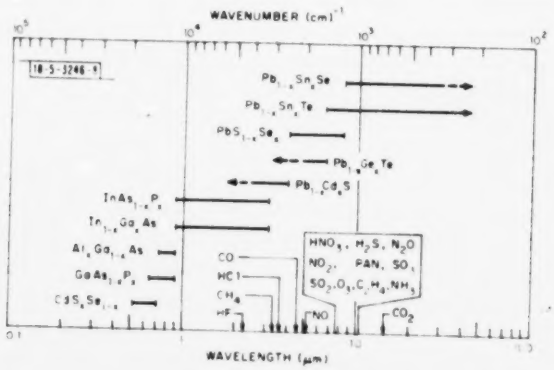

Fig. 1. Wavelength ranges which can be covered with alloyed semiconductor lasers. The arrows indicate possible further extension beyond present limits. Some of the gases of environmental concern are also shown.

(between about 2.5 and 4 μm). Principal absorbing wavelengths of some of the important pollutant gases are also indicated, at the bottom of Fig. 1. It should be noted that with these three semiconducting compounds, nearly all of the important pollutants can be detected.

Figure 2 is a drawing of a semiconductor diode laser in its standard package, approximately the same size as an average transistor. The diode crystal, nominally 0.12 × 0.05 × 0.03 cm, is mounted on a copper stud, which serves as one electrical contact. A silver ribbon serves as the other contact. Laser emission is produced by passing a current through the diode; this current can be supplied by a small battery or DC power supply for CW operation, or by a pulser for pulsed operation. There are several ways to "tune" a diode laser, the simplest being to change

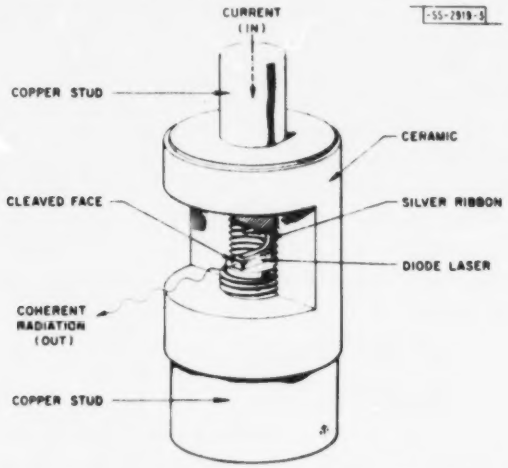

Fig. 2. Semiconductor diode laser mounted in its standard package. Over-all package size is approximately 1 cm.

the magnitude of an applied direct bias current, which changes the junction temperature through heating. Since the refractive index within the laser cavity is temperature-dependent, the laser wavelength changes. Although this type of tuning is thermal, it is still relatively fast because of the limited volume involved. Modulation frequencies of several hundred Hertz can be applied before thermal inertia becomes very noticeable, and useful experiments have been carried out with frequencies as high as 10 kHz.

1.2 Present Effort

This program is a culmination of the previous year's effort of broader scope, during which point sampling, source monitoring, and ambient air monitoring by resonance absorption were investigated, as well as remote heterodyne detection.[3] Diode lasers were developed to operate in the 1100-1200 cm^{-1} region corresponding to the ν_1 band of SO_2; its fundamental infrared band structure parameters were measured and the results published.[5]

For this year's effort, new lasers were fabricated for a selected narrow wavelength region (1120-1130 cm^{-1}) appropriate for source monitoring of SO_2, i.e., where the line strengths are strong, but relatively independent of temperature. Improvements during the year resulted in diode lasers with power levels more than ten times greater than the best achieved earlier. Various monitoring schemes were considered, and one was selected which involved a single laser

operating pulsed at two different wavelengths approximately 1 cm^{-1} apart, where the tuning of alternate pulses was accomplished by a third controllable current pulse of relatively long duration. System linearity was confirmed over a wide range of SO_2 concentrations, and the system response was also checked for day-to-day reproducibility. Measurements of interference rejection were made by using varying amounts of smoke, water vapor, steam, ammonia (NH_3), and ethylene (C_2H_4). As the program progressed, in-stack experiments were performed several times at an oil-burning power plant in order to produce information useful for final system design. At the end of the program, measurements were made at a coal-burning power plant, and the resulting SO_2 determination was compared with data obtained with a point-sampling monitor.

3. SYSTEM DESIGN

2.1 Sulfur Dioxide Absorption Spectrum

The band model and spectral line broadening parameters determined by diode laser spectroscopy in last year's program[3,5] were used to generate theoretical spectra for the entire ν_1 band of SO_2 in order to determine the optimum wavelength region for detection at temperatures to be expected in a smokestack. In Fig. 3 is a set of computer-generated scans incorporating nearly 1000 fundamental lines of SO_2, each of which had a Lorentzian profile with 0.28 cm^{-1} full-width-at-half-maximum intensity, which corresponds to atmospheric SO_2.

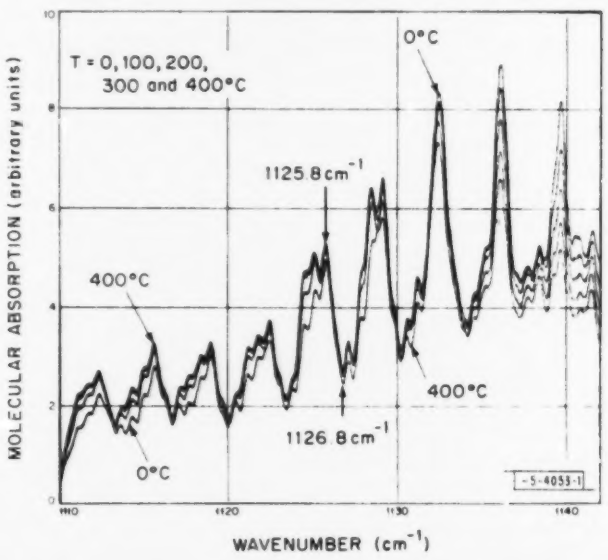

Fig. 3. Computer-generated atmospheric SO_2 absorption spectrum of a portion of the ν_1 band. The assumed linewidth was 0.28 cm^{-1} for all temperatures.

In the region of 1126 cm^{-1} there is a crossover in the temperature dependence of the absorption coefficient per molecule, so that for monitoring applications the relative temperature independence makes the 1125.8 to 1126.8 cm^{-1} wavenumber difference from "on" to "off" absorption an attractive choice. Not only would the actual in-stack measurements be relatively independent of gas temperature fluctuations with time, but of temperature variations across the stack as well.

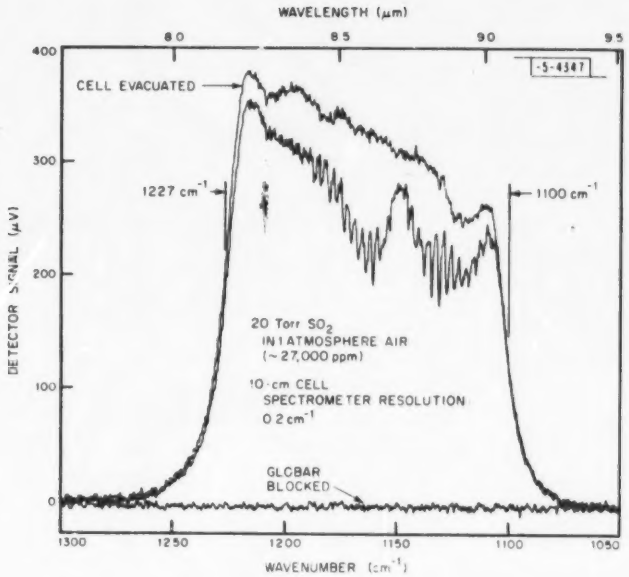

Fig. 4. Passband of infrared detector/filter combination used in stack-monitoring system.

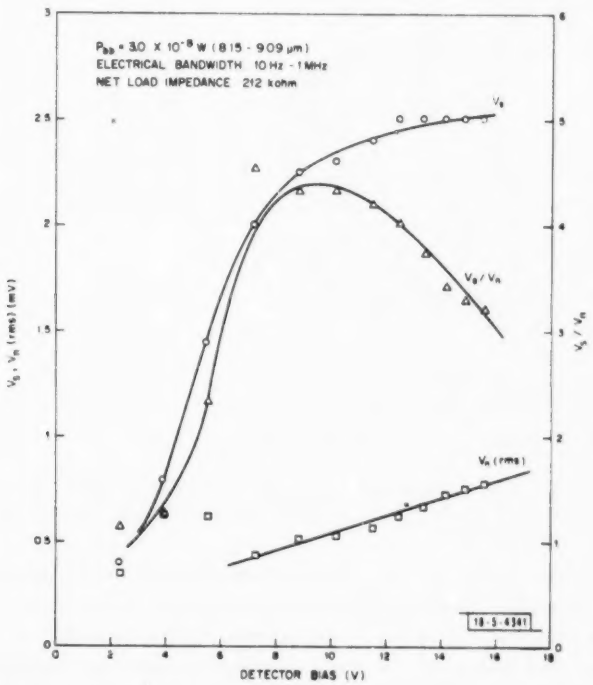
P_ab = 3.0 X 10⁻⁸ W (8.15 - 9.09 μm)
ELECTRICAL BANDWIDTH 10 Hz - 1 MHz
NET LOAD IMPEDANCE 212 kohm
Vs
Vs / Vn
Vn (rms)
Vs, Vn (rms) (mV)
Vs / Vn
DETECTOR BIAS (V)

Fig. 5. Variation in infrared detector response with bias voltage.

Detection by resonance absorption is based upon the Beer-Lambert equation

$$p = p_o \exp[-\alpha'_o cL] \exp[-\beta L] \quad , \tag{1}$$

where p_o and p are the transmitted and received laser power, respectively, α'_o is the absorption coefficient per ppm SO_2, c is the average SO_2 concentration along the path L, and β is a term defining extinction caused by turbulence, dust particles, and other substances which may be present.

If p_1 is the received power at wavelength λ_1, and p_2 the power at λ_2, then the ratio of transmitted power at the two wavelengths becomes

$$p_1/p_2 = \exp[-(\alpha'_1 - \alpha'_2)\, cL] \quad , \tag{2}$$

as long as the extinction parameter β is independent of wavelength between λ_1 and λ_2.

Since the infrared detector (to be described in the next section) is a photon counter, its output voltage is proportional to laser power, i.e., $v_1/v_2 = p_1/p_2$. If the ratio signal is analyzed by a logarithmic converter, then the output voltage is proportional to the pollutant concentration:

$$V_S = \log(v_1/v_2) = \alpha' cL \quad , \tag{3}$$

where α' $(= \alpha'_1 - \alpha'_2)$ is the effective absorption coefficient for SO_2.

2.2 Infrared Detector and Filter Assembly

The Ge:Cu detector of dimensions 2 mm × 2 mm × 3 mm was attached to the "cold-finger" of a liquid helium Dewar. In order to reduce the unwanted background radiation, a narrow-band filter was inserted in front of the detector. It is at about the same temperature as the detector (10°K).

The 1-inch-diameter filter has 85% transmission between 8.112 and 9.032 μm (1107-1023 cm^{-1}), and less than 0.1% transmission outside this region (to 13 μm). Characteristics of this detector/filter combination are shown in Fig. 4, which is a spectrometer scan over the region of interest. The passband is seen to be approximately 1 μm. For reference, a 10-cm-long cell containing 27,000 ppm SO_2 in one atmosphere of air was introduced in front of the spectrometer. This produced the SO_2 absorption spectrum noted in the figure.

Detector responsivity measurements were made with a calibrated blackbody source at 600°C, producing 3.0×10^{-8} W within the passband of the infrared filter. Using a net external load of 212 kilohms (including the 100-kilohm detector impedance, the total load is 68 kilohms), the signal voltage, noise voltage, and signal-to-noise (S/N) ratio were measured, as shown in Fig. 5. Optimum operation is seen to occur at a detector bias of around 10 volts, where S/N is a maximum. The responsivity at 10 volts bias is calculated to be 7.3×10^4 V/W. Since the total load is 68 kilohms, this may also be written as 1.1 A/W. These values for responsivity can be used to calculate the infrared power just outside the entrance window of the detector Dewar, within the passband of the filter. In detector noise calculations where power at the detector surface must be calculated, the responsivity is increased in inverse ratio of the products of the transmission of the optical elements in the Dewar: namely, the BaF_2 window (0.8) and infrared filter (0.85), producing an effective "internal" responsivity of 1.07×10^5 V/W (1.6 A/W). There is also a cold aperture in the Dewar which restricts the field of view to about 18°, or f/3.2 optics. At a detector bias of 10 volts, the noise voltage in a 1-MHz electrical bandwidth is approximately 0.5 mV. Thus, the noise-equivalent-power is 6.8×10^{-9} W.

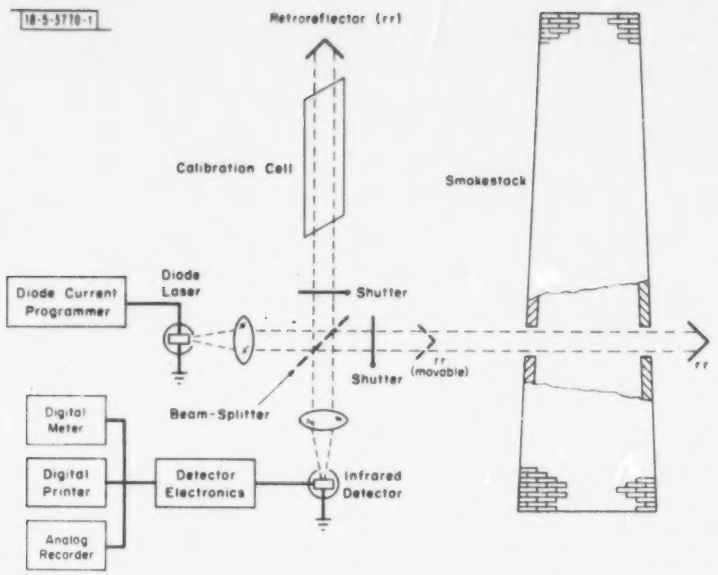

Fig. 6. Schematic of diode laser system for across-the-stack monitoring.

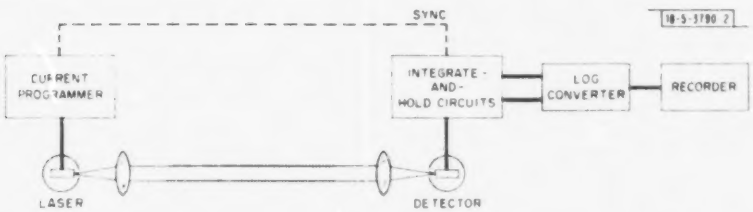

Fig. 7. Block diagram of stack-monitor operating components.

2.3 System Operation

In Fig. 6 is shown a schematic diagram of the diode-laser stack monitor. Operationally, a short (~2 μsec) pulse of current is supplied to the diode laser from the Current Programmer, causing the laser to emit radiation "on" an absorbing region of SO_2. The radiation passes through the beam-splitter and smokestack to a retroreflector situated on the opposite side of the stack; it is then reflected backward toward the beam-splitter, and onto the infrared detector. As shown in Fig. 7, the signal from the infrared detector is integrated and maintained constant so that a steady signal is fed into one side of the Logarithmic Converter. A few milliseconds after the first pulse, a low-amplitude (less than 500 mA) "tuning" current is applied to heat the junction region of the diode laser and shift its wavelength "off" the SO_2 absorption region. At the end of this "tuning" current, a second pulse is applied to the diode, whose beam traverses the same optical path as the first one. This detector signal is measured by a second Integrate-and-Hold circuit, which represents the second input to the Logarithmic Converter. The diode laser Current Programmer, Integrate-and-Hold circuits, and Logarithmic Converter have been constructed using conventional operational amplifiers, and are described in detail in Appendix A.

Figure 8 is a photograph of the entire system, consisting of the main optical table (on tripod), electronics console, analog recorder, and retroreflector (on second tripod). The tripods can be raised to a height of 12 feet above floor level. In Fig. 9 is shown a close-up view of the optical table with its plexiglass protective cover removed. Clearly visible are the tail of the diode laser Dewar and its collimating lens of BaF_2, an IRTRAN IV beam-splitter (80:20), the infrared detector Dewar and its associated lens and preamplifier, and a 10-cm-long reference cell with

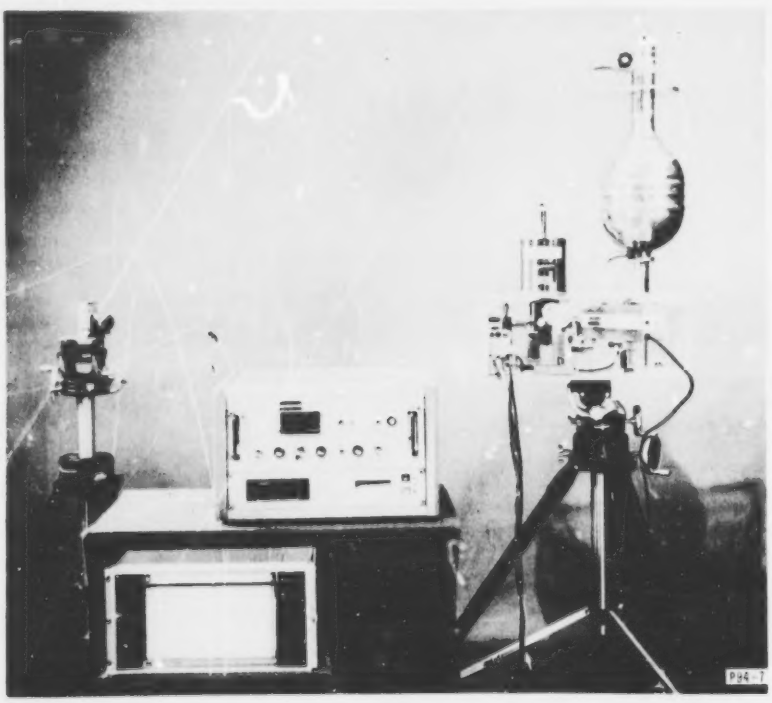

Fig. 8. Photograph of diode laser stack monitor, consisting of optical table (on tripod), electronics console, analog recorder, and retroreflector.

This page is reproduced at the back of the report by a different reproduction method to provide better detail.

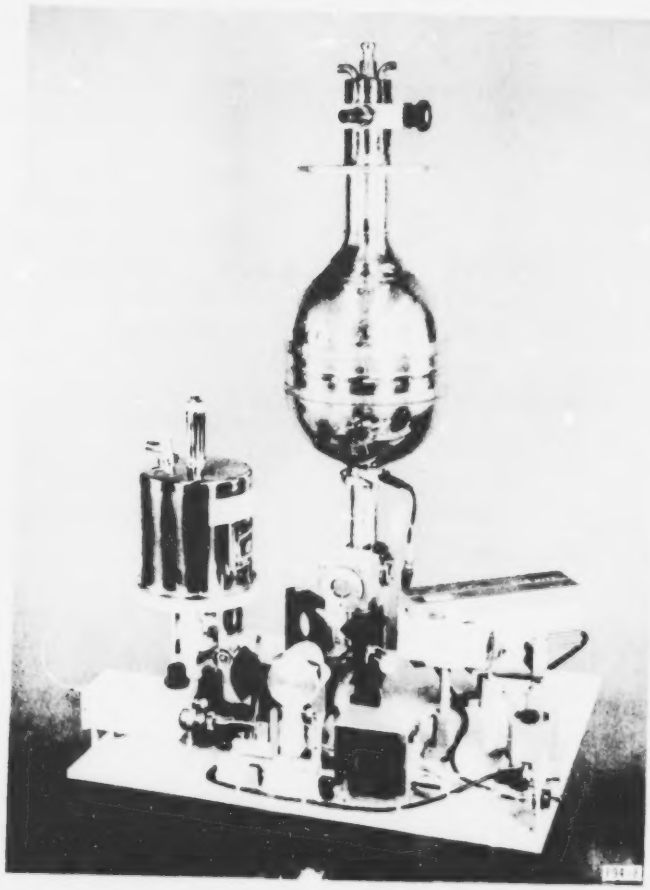

Fig. 9. Detailed view of optical table, consisting of laser and detector dewars, He-Ne alignment laser, calibration cell, beam-splitter, shutters, retroreflectors, and amplifier.

This page is reproduced at the back of the report by a different reproduction method to provide better detail.

BaF_2 windows, the He-Ne alignment laser, the beam-blocking shutters, and the retroreflector motor. The positions of the shutters and retroreflector are controllable from the main console.

The operating procedure is given in detail in Section I of Appendix A. Also contained in Appendix A are the Electronic Circuits and Timing Sequence (Section II), Electronic Alignment Procedure (Section III), and Cryogenic Dewar Preparation (Section IV).

3. DIODE LASER DEVELOPMENT

Single crystal $Pb_{1-x}Sn_xTe$ material with composition x near 0.075 was required for diode lasers emitting in the 1127 cm^{-1} region where the absorption spectrum of SO_2 is relatively independent of temperature. We discuss here various aspects of the crystal growth, material processing, and device fabrication employed during the year for optimizing the performance of $Pb_{1-x}Sn_xTe$ diodes near this composition.

3.1 Crystal Growth

Most of the growth runs were carried out using a new closed-tube, horizontal vapor growth technique. The method involves vapor growth from a metal-rich source material on $Pb_{1-x}Sn_xTe$, rather than on quartz walls as in our previously used methods. This growth technique has produced high-quality, mm-size crystals of low dislocation density. The technique (as with our earlier methods) allows growth to occur under conditions which produce p-type material with a concentration which varies with the growth temperature for temperatures above 775°C; however, because of the large diffusion coefficients at these high temperatures, the crystals grown from a metal-rich source even at 800°C are converted to n-type on cooling. By raising the growth temperature to 825-850°C, the p-type concentration of the as-grown crystals is increased and n-p junctions are formed on cooling. For growth temperatures less than 825°C, it is necessary to dope the source material with thallium (Tl), an acceptor, in order to obtain p-type material during growth and form the junction on cooling.

Although variation of growth temperature allows some control of the bulk p-type concentration, the concentration profile in the junction region is not accurately known and perhaps not as controllable as might be desired. Using junction capacitance measurements, we have found that diodes with lower threshold current densities have smaller capacitances than diodes with high thresholds. These results suggest that lower carrier concentrations near the junction region are advantageous.

In order to determine more accurately the effects of carrier density on laser performance, some annealings and subsequent diffusions of junctions at lower temperatures after the growth have been employed. We have found that the p-type concentrations which can be obtained by isothermal annealing on the Te-rich side of the stability range are apparently too large. These concentrations are generally $>10^{19}$ cm^{-3}. In order to obtain lower p-type concentrations, a two-zone annealing technique is required. This technique involves varying the vapor pressure of Te over the heated sample by placing Te in a second-temperature zone. Two-zone annealing has been used for all of the binary lead salts, but the time and temperature parameters were not known for the ternary alloys. Several annealing experiments were performed on $Pb_{0.925}Sn_{0.075}Te$ crystals, and the results showed that p-type carrier concentrations in the range of 2.3×10^{18} cm^{-3} to 10^{19} cm^{-3} can readily be achieved. However, lasers have not yet been made from two-zone annealed material.

Fabrication of lasers has continued during these annealing experiments using the junctions formed on cooling from the growth temperatures. The first lasers were made using Tl doping of the source ($\sim 10^{18}$ cm^{-3}) and relatively low growth temperatures ($\sim$750°C). Threshold current densities obtained were quite good, typically 200 mA/cm^2. However, the output power was relatively low – only a few microwatts. Since the presence of approximately 10^{18} cm^{-3} of a foreign impurity such as Tl may adversely affect laser performance, we have in recent months worked with undoped crystals.

3.2 Electrical Contacts

In addition to preparing semiconductor material for laser fabrication, an effort was made to reduce the contact resistance between the laser chip and the metal layers for contacts. This contact resistance was approximately three times that of the semiconductor itself (0.1 ohm, compared with 0.03 ohm for the average diode laser), and resulted in a significant power loss in the form of heat. Although some of this heat may be useful for current-tuning, it must be controlled to prevent thermal destruction of the laser. Most of the resistance is due to the contact to the p-type semiconductor material, for which both gold and thallium metals have been used. The lowest contact resistance (approximately 0.01 ohm) was achieved by alloying thallium to the p-type semiconductor; however, reproducibility was poor. Alloyed or plated gold contacts produce the most consistent ohmic contact to p-type PbSnTe, for which the lowest contact resistance has been about 0.05 ohm. Because of simplicity and reproducibility, plated gold contacts were used for lasers in this program.

It is important to realize that the various factors discussed here are interrelated. Alloy composition, contacting procedures, and carrier density are related in two ways, in particular, which are very important. First, variations in contacts and carrier density may affect heat production and/or heat sinking. These in turn affect the operating temperature of the device and consequently may require a slight adjustment in alloy composition to achieve the precise laser wavelength desired. Second, as the p-type concentration is lowered to obtain better thresholds, acceptably low electrical contact resistance becomes increasingly difficult to obtain.

Because of these problems, often diodes with the lowest thresholds do not emit at the optimum laser frequency or they may be limited in maximum output power by excessive heating at the contact. We believe this major difficulty can now be avoided in diodes of composition near $x = 0.075$ by employing a technique recently developed in diodes with higher SnTe composition. This technique involves diffusion after growth of a thin p^+ layer at the surface, which greatly reduces contact resistance without affecting the carrier concentration near the junction region.

3.3 Preparation of Laser Cavity

Another important advance in the fabrication technique made during the last weeks of this contract year involves polishing, rather than cleaving, the reflecting faces of the diode laser to obtain a much improved mirror quality. Up to an order of magnitude improvement in pulsed output power has been obtained by this method in otherwise identical lasers. The polishing technique has only been used on the last few devices supplied for the program.

3.4 Summary

Some test results on diodes used in the SO_2 monitoring system are summarized in the following section. These devices reflect the improvements in maximum output power which have been

obtained at the optimum laser wavelength for SO_2 absorption. Advances in fabrication techniques recently developed for other $Pb_{1-x}Sn_xTe$ compositions should result in further improvements in laser performance at this composition as well.

4. CHARACTERISTICS OF DIODE LASERS USED IN MONITORING SYSTEM

The versatility of semiconductor diode lasers permits several techniques to be considered for pollutant monitoring applications. Some of these are listed below, with comments on their suitability for in-stack monitoring.

4.1 Possible Monitoring Techniques

4.1.1 CW Laser Operation Using First-Derivative Detection

This technique is identical to that used for spectroscopic analysis of point samples at reduced pressure, with ultimate resolution limited only by the laser linewidth of around 1×10^{-4} cm^{-1}. However, the power dissipation for continuously operating diodes is normally several hundred milliwatts, which produces a substantial liquid helium "boil-off," and concomitant reduction in Dewar hold time.

4.1.2 Pulsed Operation with Two Diode Lasers

Pulsed techniques with average power levels two or more orders of magnitude below those for CW operation can reduce considerably the thermal drain on the liquid helium reservoir. Diode currents of several amperes can be used to produce high peak powers. One laser is tuned to a strongly absorbing region – the other to a region having little SO_2 absorption. Although this approach would be simple to instrument electronically, and the two diodes could be situated close together in the same Dewar, the optical alignment of the two laser beams onto a single detector would be somewhat difficult.

4.1.3 Pulsed/Current-Tuned Operation with a Single Diode Laser

This technique employs two high-current pulses separated by a tuning current, and is the one selected for the research prototype developed in this program. Initial experiments showed that the wavelengths of diode lasers under pulsed operation could be tuned at the same rate as for CW operation by the application of a steady current, or a pulse of long duration below threshold for laser action. For the stack-monitoring system, laser emission occurs when either of the high-amplitude pulses I_1 or I_2 is applied. Between the two pulses is a "tuning" current I_t of smaller amplitude (usually below threshold) but longer in duration. The sequence repeats after pulse 2, during which time the diode temperature reverts to its original value. The sequence of pulses is shown in Figs. A-5 and A-7.

The wavelength λ_1 of radiation emitted by pulse 1 (I_1) is determined by the ambient temperature of the diode laser, its chemical composition, and physical length. The emission at pulse 2 (I_2) occurs at a somewhat shorter wavelength λ_2, where the difference is a function of the diode temperature reached upon application of the tuning current. There is some shift in wavelength during I_1 and I_2 at a rate determined by the constant resistance, bulk electrical resistance, and thermal conduction of the interfaces between the laser and the liquid helium. Pulses are therefore kept as short as possible (less than 2 μsec), consistent with a reasonable signal from the infrared detector circuit, which has a time constant of 18 μsec.

Measurements were made of the pulse-to-pulse (p-p) reproducibility of laser output power by employing a current generator with 0.1% p-p repeatability. In general, the output power from the diode lasers was found to have better than 1% p-p reproducibility, which should be quite adequate for the stack-monitoring system, particularly when signals from several pulses are averaged.

4.2 Properties of Diode Lasers Used in System

Four diode lasers were incorporated into the laser Dewar, each emitting from one of four mutually orthogonal ports. This redundancy provides for three spares and also permits comparative measurements to be made. Some of their properties are given in Table I.

TABLE I

Diode	Threshold Current (mA)	Nominal IR Frequency (cm^{-1})	Total Output Power (mW)*	Absorption Due to 400 Torr-cm SO_2 at $I_t = 0$† (percent)
355	800	1121	0.2	40
376	1300	1121	1.5	32
377	1200	1122	0.6	28
379	860	1130	0.7	28

* Thermopile measurements at 2 Amp currents.

† 20 Torr SO_2 in 740 Torr air (26,300 ppm); 20-cm path length.

Three of the above devices, 376, 377, and 379, were fabricated using the new polished-cavity technique described in the preceding Section 3.3. The end faces of laser 355 were cleaved.

Since the laser is at a higher temperature for pulse 2 than for pulse 1, its emitted power during pulse 2 is generally less when $I_1 = I_2$. This is evident in Fig. 10 for these four lasers, where the output power corresponding to pulses 1 and 2 are plotted as a function of the magnitude of the tuning current. As expected, the power emitted by I_1 is relatively independent of tuning current, since the laser had been able to return to its original temperature beforehand. This is clearly not the case for I_2; consequently, there must be a provision for adjustment of the pulse amplitudes or widths in order to have identical "untuned" and "tuned" transmissions in the absence of SO_2. For this prototype system, a potentiometer on the front panel controls the duration of I_1 to permit equalization of signals.

While Fig. 10 represents the output power of the diode lasers for a range of tuning currents, the ratio of the output powers at pulses 1 and 2 is used to measure the SO_2 concentration, provided that the equalizing adjustment has been made at a particular value of I_t. The effective absorption coefficient per ppm SO_2, α', was determined by alternately filling the 10-cm calibration cell with 20 Torr SO_2 in 740 Torr air, and evacuating the cell. The results are shown in Figs. 11(a) through (d) as a function of the tuning current. It is important to note that there is a systematic and reproducible dependence of α' on tuning current from day to day, depending on the manner in which the laser Dewar was filled with liquid helium (see Appendix A, Section IV). This difference in "tuning" response between "direct" fill and "precooled" fill is particularly evident in Fig. 11(b) for diode 376, and presumably arises from a small change in thermal conduction between the liquid helium and the Dewar tail using the two techniques of filling. Even

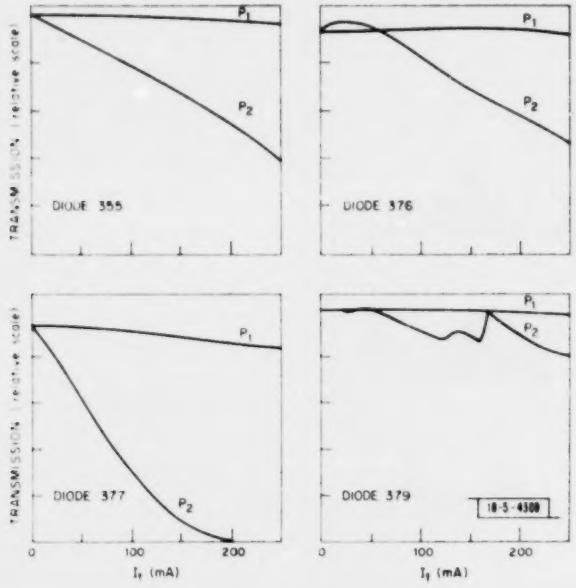

Fig. 10. Variation of output laser power with tuning current for the four diodes used in the stack-monitoring system. p_1 and p_2 refer to emitted power by currents I_1 and I_2 (tuned), respectively.

when the same fill procedure is used, there are minor differences in "tuning" response caused by changes in the thermal properties of the diodes under temperature cycling. Therefore, recalibration is necessary each time the laser is cooled from room temperature to its operating temperature. If the low temperature is maintained, however, the "tuning" response is constant and no recalibration should be necessary.

From Eq. (3) it can be shown that the effective absorption coefficient per ppm SO_2 can be deduced from the expression

$$\alpha' = \alpha'_1 - \alpha'_2 = \frac{V_S}{GcL} \quad , \tag{4}$$

where α'_1 and α'_2 correspond to absorption at pulses 1 and 2, respectively, and V_S is the output voltage from the ratio gain control circuit, as monitored on the analog recorder or digital panel meter. G is the voltage gain beyond the log converter, c is the SO_2 concentration in ppm, and L is the path length in cm.

In selecting an appropriate tuning current for a particular diode laser, a high α' is desired at the lowest usable tuning current (in order to minimize liquid helium boil-off). There is another consideration to be made, however, related to the laser power itself. If detector noise is the determining factor for ultimate sensitivity, as it is in the laboratory, then for two lasers with the same α', that one with higher power will have a greater detection capability. Recall from Eqs. (3) and (4) that the output voltage can be written as

$$V_S = G \ln\left(\frac{V_1}{V_2}\right) = G\alpha' cL \quad . \tag{5}$$

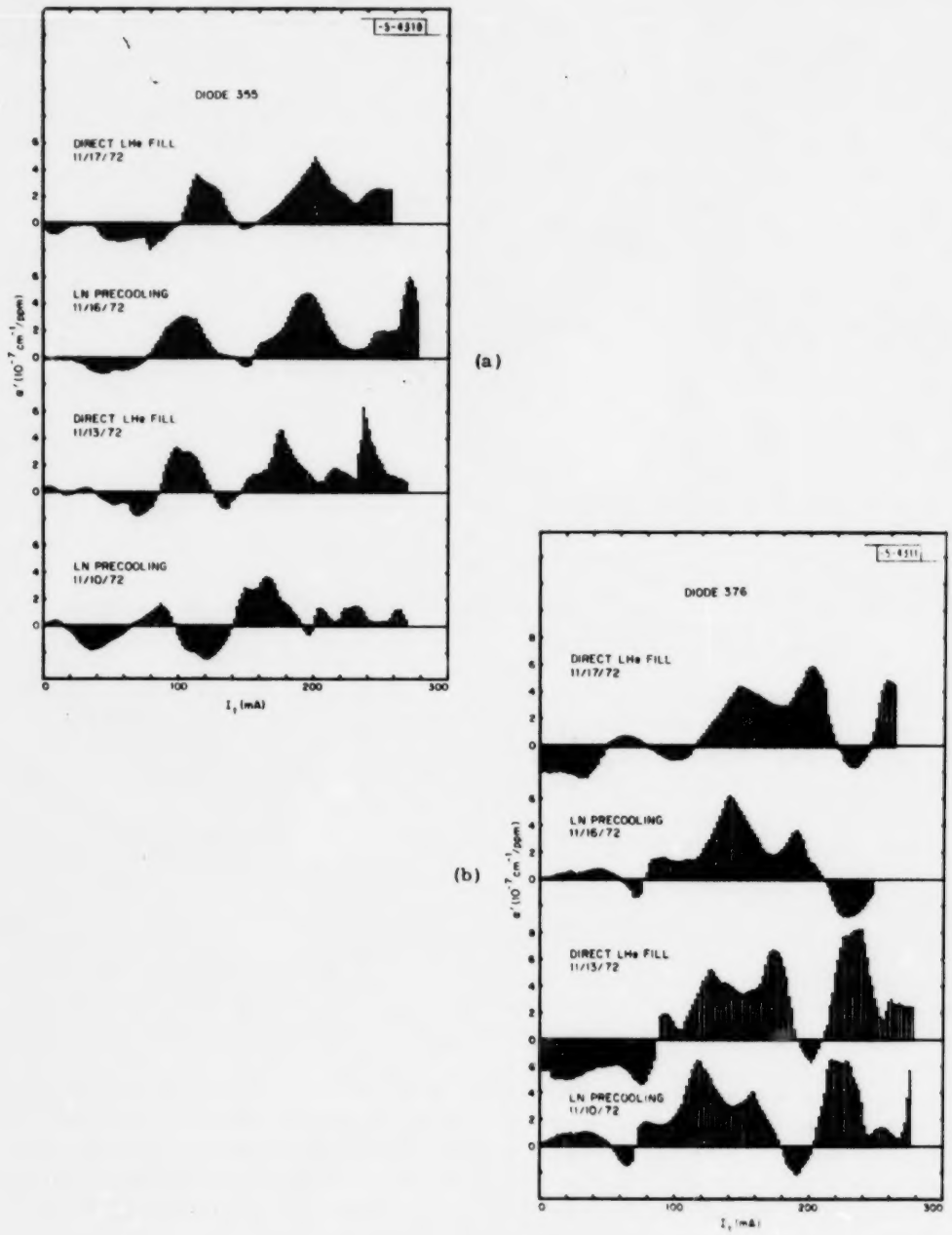

Fig. 11(a-d). Effective SO_2 absorption coefficient vs tuning current for the four system diode lasers, illustrating variations caused by different LHe fill procedures.

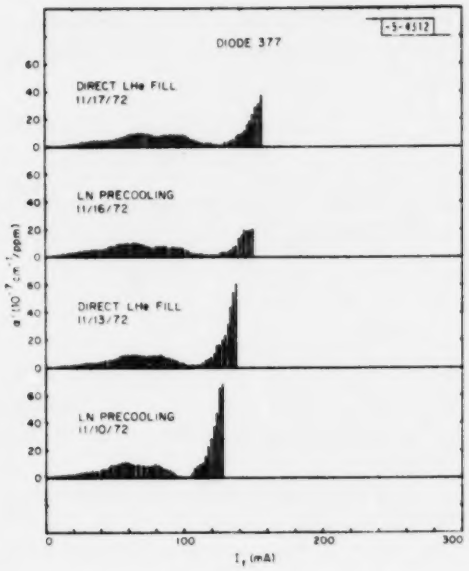

(c)

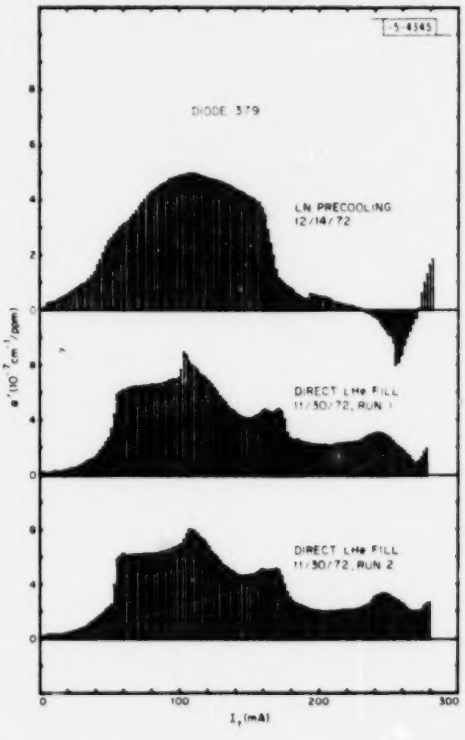

(d)

Fig. 11. Continued.

where V_1 and V_2 are the infrared detector voltages due to I_1 and I_2, respectively. If V_n is a detector noise component present in both V_1 and V_2, and V_N the output noise due to this term, then

$$V_N \cong \left[\left(\frac{\partial V_S}{\partial V_1}\right)^2 + \left(\frac{\partial V_S}{\partial V_2}\right)^2\right]^{1/2} V_n \quad . \tag{6}$$

Consequently, for a particular concentration c of SO_2, a fixed pathlength L, and a detector noise voltage V_n, the output signal-to-noise ratio becomes

$$\frac{V_S}{V_N} \cong \left(\frac{cL}{\sqrt{2}V_n}\right) \alpha' V_{1,2} \quad . \tag{7}$$

where $V_{1,2} \cong V_1$ or V_2. It is clear from Eq. (7) that it is the product $\alpha' p_o$ which determines the signal-to-noise ratio under these conditions, since $V_{1,2}$ is proportional to the laser power p_o. Consequently, that diode having the largest $\alpha' p_o$ product will have the best SO_2 detection capability.

Figure 12 supports the above analysis. In this figure are plotted the signal-to-noise ratios for six different diode lasers for the detection of 20 Torr SO_2 in 740 Torr air over a 20-cm path. The signal-to-noise ratios range from 2.5 (for diode 375 at I_t = 84 mA) to 108 (for diode 379 at

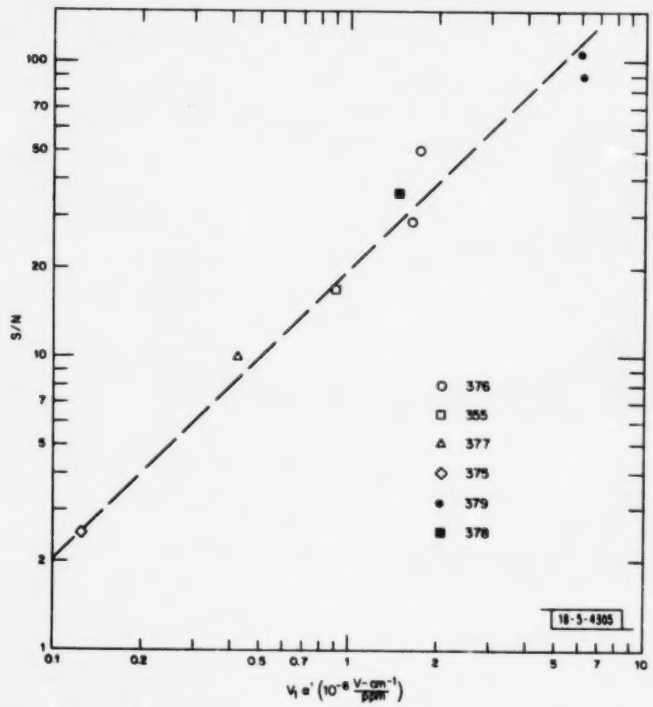

Fig. 12. Signal-to-noise ratios for six different diode lasers in the detection of 20 Torr SO_2 in 740 Torr air over a 20-cm path. The noise values used were peak-to-peak fluctuations with 0.3-sec averaging.

66 mA). The noise represents peak-to-peak fluctuations with 0.3-second averaging. If the rms value had been used, the signal-to-noise values would be 2 $\sqrt{2}$ times larger, ranging from 7 to 305.

For actual operation in the field, other (external) factors will probably limit sensitivity of the system. If the noise term in this case is defined as N_{ext}, then the signal-to-noise ratio becomes

$$\frac{V_S}{V_N} = \frac{G\alpha' cL}{N_{ext}} \quad . \tag{8}$$

The laser power is unimportant as long as N_{ext} is substantially larger than the detector noise contribution, and the absorption coefficient α' is paramount. In other words, lasers with higher output power levels would not improve the detection sensitivity.

Other considerations, such as possible interferences with other constituents, and linearity under different conditions, will be considered in Section 5.

5. LABORATORY TESTS

Tests were performed in the laboratory in order to determine sensitivity, linearity, and interference characteristics of the diode laser system operated according to the procedure described in Section 2 and Appendix A.

5.1 Sensitivity

Figure 12 of the preceding section was used to illustrate the laser parameters important for sensitive detection of SO_2. The signal-to-noise data were for the detection of 20 Torr of SO_2 in 740 Torr air (26,300 ppm) over a pathlength of 20 cm. For comparison purposes, the equivalent concentration for two-way transmission across a smokestack 5 meters in diameter is 526 ppm. For diode 379, the signal-to-noise ratio for detection of this equivalent concentration is approximately 100 for a 0.3-second averaging time. Recall that the noise represents a peak-to-peak variation; consequently, if we assume that a signal-to-noise ratio of 2 is appropriate for defining the ultimate detection sensitivity (this would correspond to S/N = 5.6 for rms noise), the minimum detectable concentration of SO_2 is around 10 ppm for this particular diode, with 0.3-second averaging. Mathematically, this result may be written as

$$c_{min} \approx \frac{5}{\sqrt{T}} \text{ ppm} \quad , \tag{9}$$

where T is the integration (or averaging) time in seconds, as set by the selector switch on the front panel of the electronics console. If very fast response is not needed, a time constant of 10 seconds can be used, such that the minimum detectable concentration becomes 1.7 ppm.

Some final observations should be made with regard to the above analysis. First, under actual stack-monitoring conditions, fluctuations in the transmitted power at wavelengths λ_1 and λ_2 will occur as a result of turbulence and particulate scattering within the stack. Although such effects are partially canceled by the ratio technique, they are not eliminated entirely. If the purpose of this system were to provide the long-term, steady monitoring capability of an instrument ready for the production line, then time constants of many minutes would have been incorporated. However, since its main purpose is to investigate a principle involving infrared laser technique for in situ monitoring, the shorter time constants provide the means of investigating rapid fluctuations, which may be caused in part by temporal variations in the SO_2 concentration

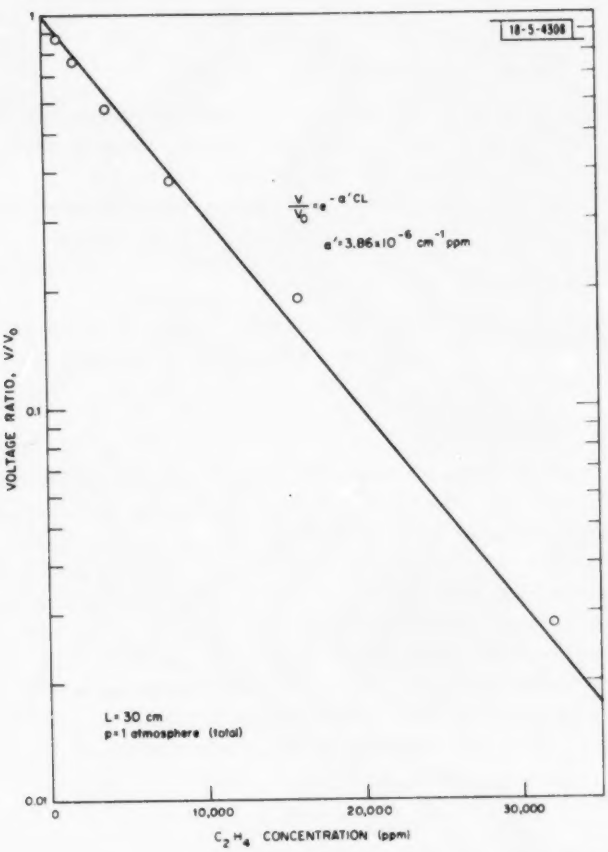

Fig. 13. Linearity check of integrator-log converter combination, using a 10.6-μm diode laser (single-wavelength) and varying concentrations of atmospheric C_2H_4.

as well as by the other factors mentioned above. The extent to which Eq. (9) holds for the field measurements will depend upon these factors, and it must be recognized as an upper limit of sensitivity for that particular diode laser. The other lasers will have minimum detection limits proportional to the signal-to-noise values in Fig. 12.

5.2 Linearity

5.2.1 Confirmation of the Beer-Lambert Equation

During the early stages of this program, measurements were made of the pulsed-laser transmission through a 30-cm-long cell containing ethylene (C_2H_4) of varying concentrations in one atmosphere of air, using an available diode laser operating in the 10-μm region. The purpose of this experiment was to verify the equation, $p = p_o \exp[-\alpha' cL]$, introduced earlier, over a wide range of concentrations, and thereby validate our assumptions on which electronic design of the prototype SO_2 monitoring system was to be based.

Figure 13 shows the relative transmission (I/I_o) as a function of C_2H_4 concentrations from zero to 32,000 ppm. The straight line is a theoretical fit to the data corresponding to an α' of a 3.86×10^{-6} cm^{-1}/ppm. Using a 0.1-second post-detection time constant, the effective noise level was found to be 19 ppm for this experiment with a 30-cm cell, and was caused by the detector noise only.

5.2.2 Linearity for the Two-Pulse (Ratio) Technique

In order to determine linearity of the technique incorporating the ratio of transmissions corresponding to two different wavelengths, λ_1 and λ_2, of the laser radiation, for concentrations to be expected in a working smokestack, a diode laser emitting around 8.9 μm was adjusted for optimal values of pulse and tuning currents. The effective absorption coefficient α' ($= \alpha'_1 - \alpha'_2$) was 2.3×10^{-7} cm^{-1}/ppm SO_2. Concentrations for a 10-meter-diameter stack were simulated in a 1-meter cell by increasing the SO_2 values tenfold.

The result of this study is shown in Fig. 14 for SO_2 concentrations ranging from 100 to 2000 ppm. The output voltage from the logarithmic converter is seen to be essentially linear with respect to the SO_2 concentration, as expected.

In order to demonstrate linearity of the system at a variety of tuning currents for a particular diode, the above experiment was repeated for laser 379 at tuning currents of 40, 100, 140, 170, 200, and 230 mA, each of which represents a local peak or valley for absorption. The data for this diode are plotted in Fig. 15 for SO_2 concentrations to 500 ppm (along a 10-meter effective path), and show good linearity at each value of tuning current.

5.3 Interferences Due to Smoke, Water Vapor, and Steam

A specimen of gas from a nearby oil-fired stack was obtained and analyzed in the 730-cm-long White cell constructed during last year's program. The object was to determine the SO_2 concentration and observe any interference effects which may be revealed by a high-resolution laser scan of the stack gas at reduced pressure. By placing a small modulation current on the steady diode current, derivative spectra were obtained. The stack-gas scan is shown in Fig. 16, together with one for pure SO_2. By comparing the two traces, we determined that the stack gas contained 670 ppm SO_2. Moreover, it is clear from the spectra that there are no strong interferences over this wavelength region due to any other gases. Although these particular SO_2 lines are about 20 times weaker than the strongest lines observed, the noise level is adequate

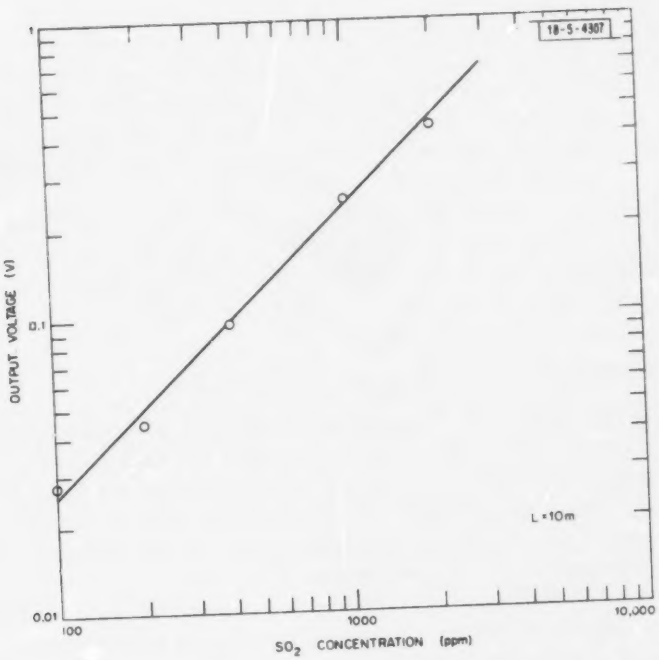

Fig. 14. Linearity check of ratio (two-pulse) technique for the detection of SO_2 in the 8.9-μm region. Equivalent concentrations for a 10-m path were achieved by a tenfold increase of the SO_2 partial pressure in the 1-m path used for this test.

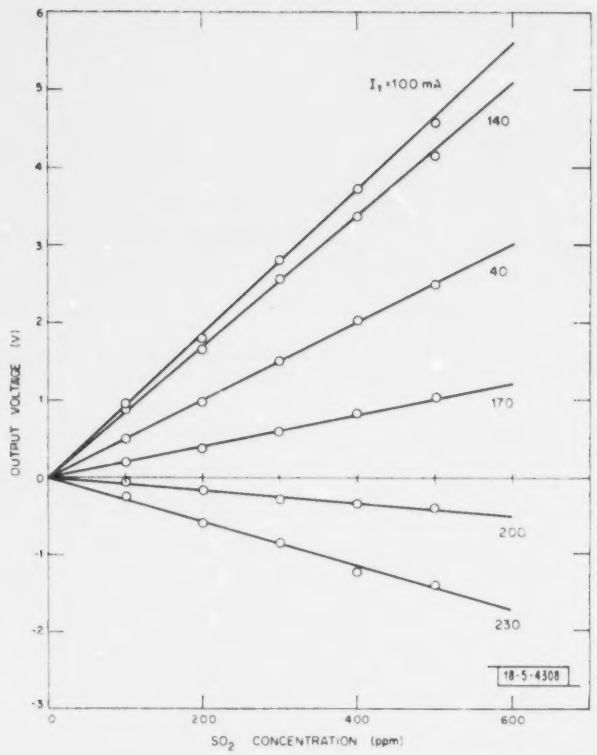

Fig. 15. Linearity check of ratio (two-wavelength) technique for the detection of SO_2 at various diode laser tuning currents, from 100 to 230 mA. The output voltage is positive or negative, depending on the position of the nominal (untuned) wavelength relative to the SO_2 absorption lines.

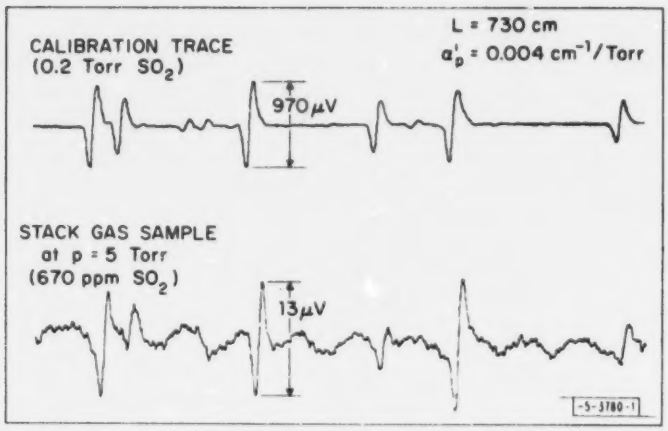

Fig. 16. Derivative detection scan for SO_2 in a specimen of stack gas. Laser modulation current was approximately 1 mA peak-to-peak.

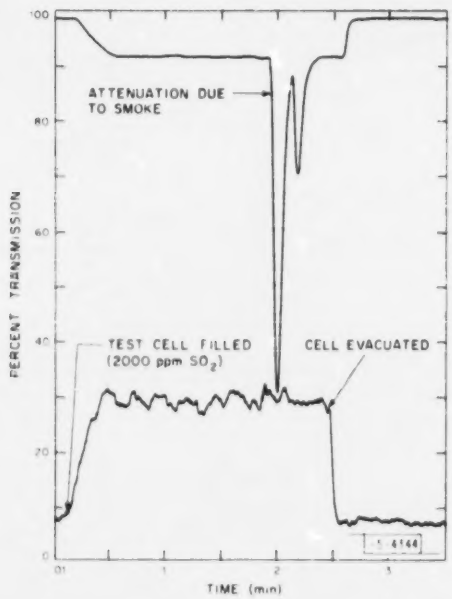

Fig. 17. Interference effect of smoke on SO_2 determination. The lower curve is the SO_2 (ratio) signal, on an arbitrary linear scale.

at 20 ppm. (Had the laser wavelength been in the region of the strongest SO_2 absorption line, the equivalent noise level would be 1 ppm under the same conditions.) The periodic, slowly varying oscillations throughout the stack-gas scan are caused by reflections between the entrance and exit windows of the White cell (Fabry-Perot effect).

The lack of interfering gases shown by the above measurement suggests that water vapor will probably be the major contributor to absorption and scattering losses, particularly when scrubbers are being used. Although the 1127 cm^{-1} region is well-placed between relatively weak water vapor lines, it is known that at atmospheric pressure the "wings" of such lines can extend unusually far from the line centers. In order to observe the effects of smoke, water vapor, and steam on the system, a 20-cm-long pyrex tube (open at both ends) was placed in the diode laser beam. (For the steam test, the walls were heated above 100°C.) The tube could be filled by a port at the center, with discharge from both ends. Also along the laser beam was placed a closed 10-cm-long cell filled with a mixture of SO_2 and air at atmospheric pressure. The effect of smoke attenuation is illustrated in Fig. 17. The upper trace corresponds to transmission of pulse 2, whereas the lower trace is the ratio of transmissions at λ_1 and λ_2. No noticeable change in the SO_2 reading is produced for up to 60% attenuation of the laser beam.

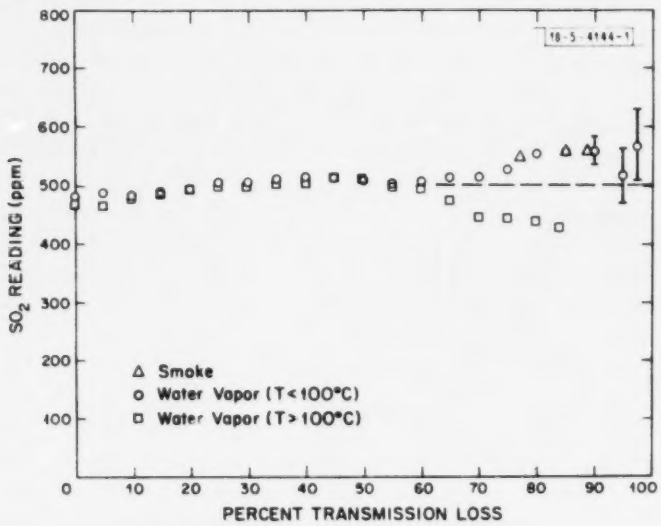

Fig. 18. Interference effects of smoke, water vapor, and steam on SO_2.

Attenuation due to any of the above sources can be as high as 65% before there is a significant change in the SO_2 reading. This is illustrated in Fig. 18 where in one case the absorption ranged from zero to 98%. It is evident that the water vapor interferes as an aerosol (similar to the smoke), while the steam interference is probably due to infrared absorption.

5.4 Interferences Due to Other Gases: NH_3, C_2H_4

Each of the four diode lasers incorporated into the final system was checked for responsivity to NH_3 and C_2H_4, in addition to SO_2. Since NH_3 is used as a wavelength calibration standard in the 8.9-μm region, some interfering regions were expected.

The results of the gaseous interference tests are shown in Figs. 19(a) through (d). In each case, the effective absorption coefficient (per ppm) for SO_2 is indicated by the solid line, for NH_3 by the plus signs, and for C_2H_4 by the dotted line. Regions of tuning current for sensitive detection of a particular gas are readily apparent. For example, for diode 355 a tuning current of 18 mA produces an α' of 1×10^{-7} cm^{-1}/ppm for SO_2, with no interference from either NH_3 or C_2H_4. Diode 376 shows better response to NH_3 than to SO_2 or C_2H_4 over most of its tuning range, with an absorption coefficient of 8×10^{-7} cm^{-1}/ppm at a tuning current of 40 mA. It is clear that for the conditions under which this diode was operated (pulse width of 3 μsec), SO_2 could not be detected in the presence of NH_3, unless correlation readings were taken at two or more values of tuning current. (The NH_3 interference is positive below 100 mA, and negative above.) For diode 377, Fig. 19(c) indicates specific SO_2 detection at around 30 mA. Diode 379 is sensitive only to SO_2 for tuning currents to 140 mA, with an average absorption coefficient of 2×10^{-7} cm^{-1}/ppm. As indicated in Section 5.1, the combination of high power and strong absorption coefficient makes this diode the best of the four for monitoring SO_2.

The interferences shown in Figs. 19(a) through (d) can be minimized if the laser current pulse widths are reduced below the value used for these tests (3 μsec). The amount of laser frequency "chirping" is approximately 0.1 cm^{-1} per μsec pulse width, although the exact variation depends on the particular laser. Ideally, the pulse width should be less than 0.1 μsec to detect atmospheric gases; however, since the detector time constant is 18 μsec, such short pulses produce very weak signals. In order to confirm this relationship between pulse width and specificity, these interference experiments should be repeated using different laser current pulse widths.

Interferences from many other gaseous constituents present in smokestack effluent, such as CO and NO, can be ruled out because they do not absorb around 8.9 μm. Although the tuning range of the two-wavelength technique is less than 0.1% of the nominal infrared frequency, there may be interferences from other constituents; this will have to be checked by further studies. Ultimately, high-resolution laser scans of stack-gas samples in regions covered by the pulsed lasers during field operation would afford the best assurance that there are no significant interferences.

6. FIELD TESTS

6.1 Helium-Neon Laser Transmission Across an Oil-Burning Stack

In order to design an optical system for in-stack monitoring of SO_2, it was deemed important to measure the transmission properties of a visible laser beam through a typical stack (broadening of image due to thermal convection currents, translation of image position, scattering, absorption, etc.). A 1-mW He-Ne laser, operating in the visible at 0.6328 μm, was used to perform this experiment. The laser beam was directed through a stack at the Air Force Cambridge Research Laboratories having an inside diameter of 2.45 meters. The distance from laser to ground-glass/Polaroid film camera detector system was 3.2 meters. Photographs were made to show the image size, degree of sharpness, and position during both quiescent and stack-purging conditions. The photographs of Fig. 20 were taken with Polaroid 3000-speed film at a camera setting of f/16 for 0.1 second.

As shown in Fig. 20(a), where the laser beam was transmitted over a 3.2-meter path in the laboratory, the undisturbed image is sharp, with a diameter of 0.32 ± 0.02 cm. During quiescent (normal) operation of the stack, it is clear from Fig. 20(b) that some blurring of the image has occurred (presumably due to temporal variations in refractive index caused by convective currents

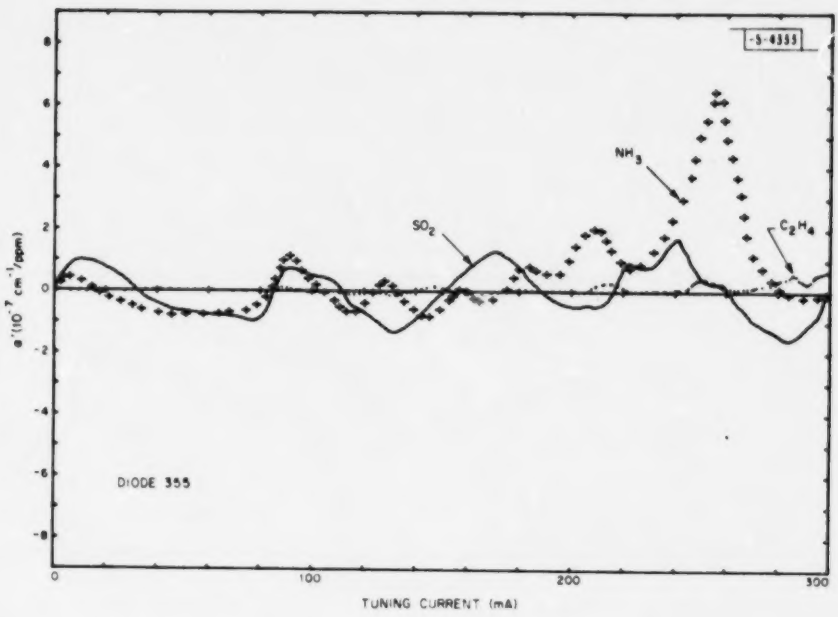

(a)

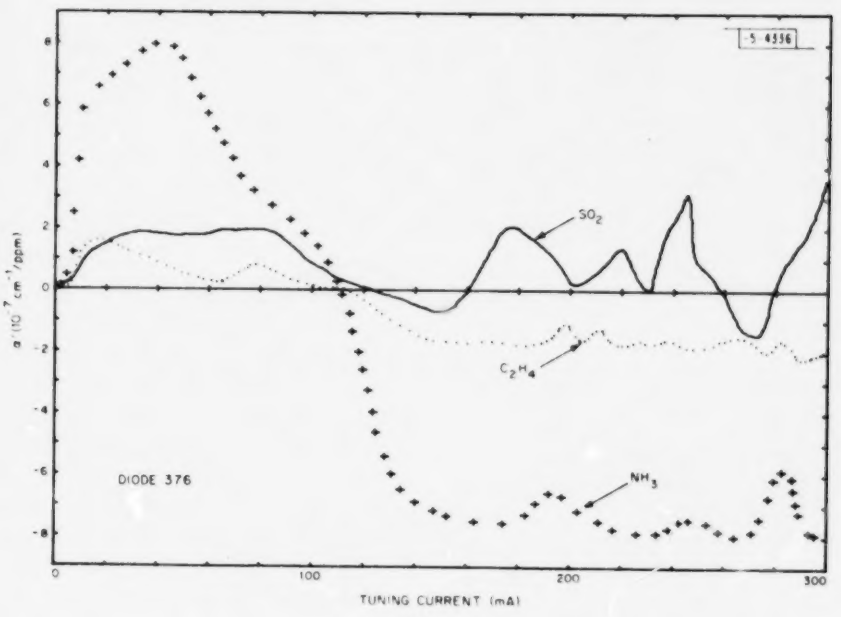

(b)

Fig. 19(a-d). Interference of other gases: Sensitivity of four system diode lasers to SO_2, NH_3, C_2H_4 for various tuning currents.

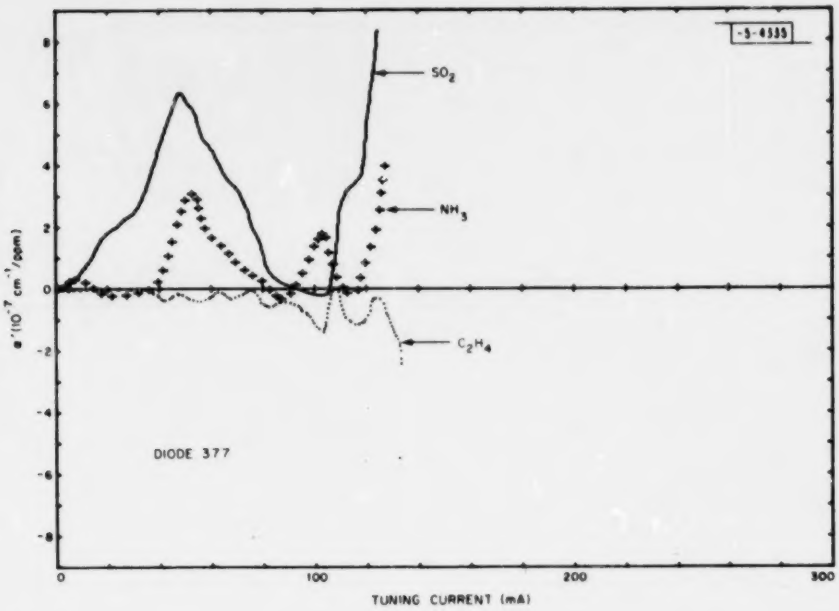

(c)

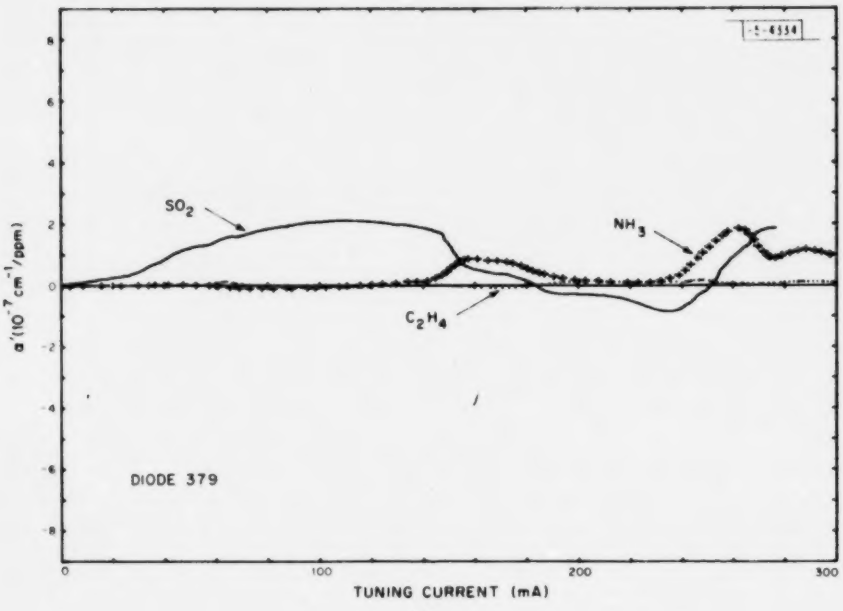

(d)

Fig. 19. Continued.

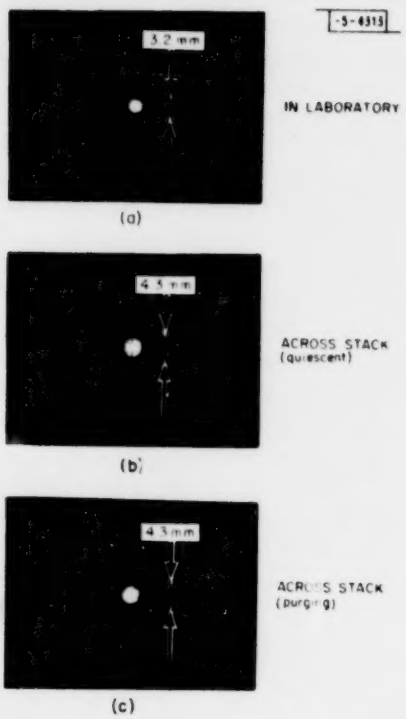

Fig. 20. Photographs of He-He laser beam after being transmitted across a smokestack 2.45-m wide. Total beam path was 3.2 m.

in the effluent), and its diameter has increased by 0.11 cm to 0.43 ± 0.03 cm. When the stack was purged to release collected particulates from the boiler, no significant change was observed in either the intensity or the size of the laser image, although there was an apparent translation of the beam by approximately 0.2 cm, as shown in Fig. 20(c). (The "translation" may have been partially caused by deflections of the walls on which the laser and camera were mounted.)

If we extrapolate these results for a 2.45-meter-diameter stack to one whose diameter is 10 meters, the size increase and position shift for a one-way pass will be about four times larger, or 0.44 cm and 0.8 cm, respectively. (Since scattering should be significantly less at 8.7 μm than at the 0.6328-μm wavelength used in this experiment, the effect here is probably larger than it will actually be.) Assuming such a 0.8-cm translation in the beam (1.6 cm for a two-way path), the effective deviation in direction from the undistorted beam is approximately 0.05°. A 3.8-cm-diameter collecting lens with a focal length of 10.6 cm, together with an infrared detector of 0.05-cm diameter, yielding a collecting angle of 0.3°, should be adequate.

6.2 In-Stack Measurements (Oil/Natural Gas) Using Diode Laser

Using a $Pb_{0.93}Sn_{0.07}Te$ diode laser emitting around 8.9 μm, tests were again made at the AFCRL stack to obtain operational information prior to final system design. The ambient temperature outside the stack where the electronics system was located was high (115 to 120°F), and the relative humidity was 35%. The fuel was No. 6 grade oil containing 1.43% sulfur, consumed at a rate of 430 to 460 gal/hr. Two boilers were operational, and the stack-gas temperature was approximately 470°F (243°C). During the experiments, conversion was made from natural gas to oil, and back to gas.

Single-pass attenuation of the diode laser power by the stack gases and particulates was less than 10%. However, with the infrared detector situated near one of the ports, infrared emission from the hot gases produced "noise" several times larger than the inherent detector noise. The detector voltage shown in Fig. 21 corresponds to three conditions: (a) detector looking through the stack at the "cold" laser (diode current zero), (b) same conditions as (a), except that the laser Dewar was blocked from the detector field of view, (c) stack blocked from detector field of view (detector noise limit). By comparing Figs. 21(a) and (b), it is clear that the noise contribution due to random fluctuations of the position of the "cold" object (laser package) was small. Most of the noise was caused by the stack gases themselves, the dominant frequency being approximately 50 Hz. Because of the infrared filter, the detector responds only to radiation between 1100 and 1227 cm^{-1} (see Fig. 4); consequently, the wideband thermal radiation responsible for the noise in Figs. 21(a) and (b) must be within this wavelength region. Since, ideally, the detector noise of Fig. 21(c) should represent the limiting sensitivity, steps had to be taken to reduce

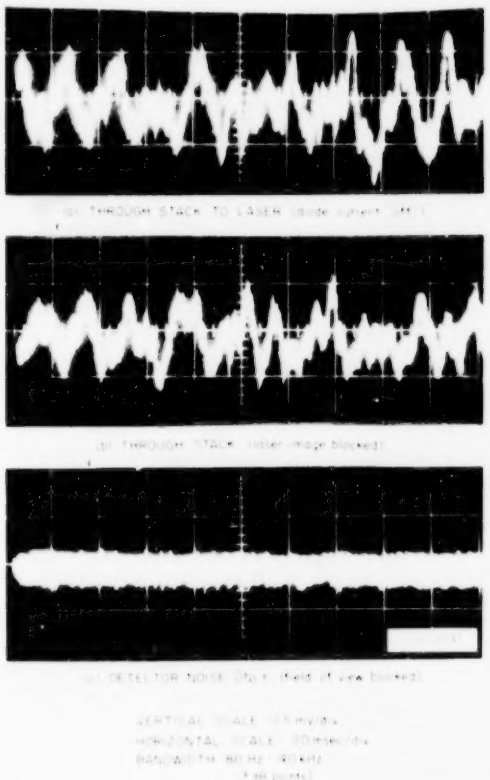

Fig. 21. Infrared detector signal during stack monitoring under different conditions: (a) Through stack to laser, with laser current "off"; (b) through stack, but laser image blocked; (c) detector blocked so that it does not "see" the stack at all. Vertical scale: 0.5 mV/div; horizontal scale: 20 msec/div. Bandwidth (3-dB points): 80 Hz to 40 kHz.

stack-gas "noise" from its value of 1 mV (peak-to-peak) to below the 0.25-mV value of the detector itself. There were several ways to accomplish this:

(1) Reduce optical bandwidth even further.
(2) Use a high-pass electrical filter to eliminate the low-frequency "noise."
(3) Increase system integration time.
(4) Utilize unsymmetrical transmission/reflection characteristics of beam-splitter so that only a small fraction of the stack-gas emission is collected by the infrared detector (this is possible for the two-way transmission technique shown in Fig. 6).

The following corrective action was taken to reduce the fluctuations in the infrared detector signal induced by the stack gases.

(1) A second infrared filter was ordered, which would block transmission above 1142 cm^{-1}. In conjunction with the 1100-1227 cm^{-1} filter already installed, the combined effect would be to reduce "noise" due to stack gases at 250°C by a factor of 3.6, and the laser signal by 25%. However, because insertion of this filter involved redesign of the detector package, and because of the uncertainties associated with transmission through two filters in series, we decided not to incorporate this new filter unless absolutely necessary.

(2) The coupling capacitor between the infrared detector and preamplifier was reduced from 1 microfarad to 0.001 microfarad, raising the minimum detectable frequency to 140 Hz. Since the dominant frequency of the stack-gas-induced "noise" was 50 Hz, this modification resulted in a 70% reduction, with no effect on the 2-μsec-wide laser pulses.

(3) New circuits were designed and incorporated into the system to permit the selection of integration times from 0.1 second to 10 seconds at the output stages of both "transmission" and "SO_2" readings.

(4) The optical table was designed to permit the return signal for two-way transmission to reflect off (rather than be transmitted through) the beam-splitter. As a result, only 20% of the stack-gas radiation is collected by the infrared detector, with no effect on the laser pulse.

During these initial field measurements, conversion was made from oil to natural gas. Measurements made during this conversion are shown in Fig. 22, where the upper trace represents the transmission across the stack, which increased by a few percent after conversion. Although the diode laser was not optimally tuned to monitor the SO_2 concentration during this experiment, there was a detectable reduction in the SO_2 content during the shift from oil to natural gas. The large spikes probably stem from higher SO_2 concentrations produced when the gas flame oxidized unburned sulfur which had collected on the walls of the furnaces.

After making these improvements, the system was assembled for two-pass operation at the same facility. The optical table was placed on the floor (rather than on a tall tripod at the access port) and two plane front-surface mirrors were used to direct the laser beam to the port, approximately 12 feet high. Another mirror was positioned at the other side of the stack, and was also supported by a tripod.

As a result of the improvements made since the first field test with a diode laser, the optical alignment procedure was simpler and "noise" induced by the stack gases was absent. Without

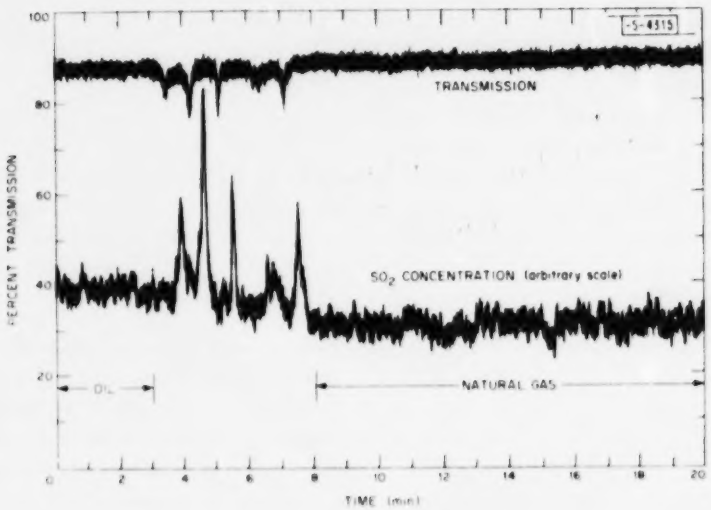

Fig. 22. Measurements of transmission and SO_2 concentration made during conversion of power plant from oil to natural gas. Stack diameter: 2.45 m.

any adjustments, internal calibration at the stack site agreed with that obtained earlier in the laboratory for the 1000-ppm internal "calibration" cell, although the "zero" setting was 60 ppm high. It should be noted that during the one and a half hour period between laboratory checkout and assembly at the field site, the laser and detector Dewars were dismantled, electronics deactivated, and transport of the components carried out.

With the function switch set to the "Monitor" position, the laser beam was directed from floor level to the mirror at the access port to the stack (a distance of 12 feet), through the 2.45-meter (8-foot) stack to the reflecting mirror, back through the stack, and down to floor level again. The net transmission over the two-way path was 80%, in agreement with earlier measurements which indicated 90% transmission for the one-way configuration. Unfortunately, the return signal suffered fluctuations of as much as 90%, caused by deflection of the beam by the turbulent gases in the stack and the long moment arm of this arrangement. Using a 3-second post-detection time constant, the fluctuations in the transmitted signal were reduced so that transmission could be read to ±1.5%.

Since the SO_2 signal is determined by the ratio of adjacent transmitted pulses, the large signal fluctuations made the SO_2 reading very noisy, and difficult to interpret. (Post-detection filtering of the ratio signal comes after the logarithmic converter, so that all of the transmission noise is at its input.) As a calibration check, a 30-cm-long cell containing 3120 ppm SO_2 was inserted into the path of the laser beam. The SO_2 reading was found to increase by 3200 ppm. When the calibration cell was removed, we noted that the average SO_2 signal varied over a range of 250 ppm every few seconds. Although this variation probably corresponds to changes in the SO_2 content of the stack gas, there was uncertainty as to the actual location of zero ppm on the recorder, so that the absolute value could not be obtained.

6.3 On-Line SO_2 and Transmission Measurements at a Coal-Burning Power Plant

Final measurements were performed in Worcester, Massachusetts at the Webster Street Station of the Massachusetts Electric Company. The full load capacity of the power station was 35 megawatts, produced primarily by bituminous coal (16-17 tons per hour), although some oil was being used to reduce particulate emissions. The coal contained 0.8% sulfur, and air atomization was used in the furnace. An Aerotech Cyclone dust precipitator was in operation.

The diode laser system was transported to the site and positioned so that the beam traversed a 5-meter-wide horizontal breech between the precipitator and fans which forced the combustion products into the stack. Caps were removed from 4-inch-diameter pipes to permit optical transmission directly across the breech; and, because the apparatus was located before the exhaust fans, a negative pressure existed which eliminated the need for windows. Another port was available for the insertion of a Dynascience SO_2/NO_x point sampling monitor, operated by Charles Rodes of the Environmental Protection Agency.

The high particulate loading of this stack (2.5 grains per cubic foot) together with the long optical path attenuated the laser signal by 99% when the two-way configuration shown in Fig. 6 was used. Under these conditions, the signal was only a few times larger than the detector noise, so that the ratio signal proportional to the SO_2 content was too noisy to be meaningful. By placing the detector Dewar on the opposite side of the stack, for single-path transmission, the transmitted signal was an order of magnitude higher, and it was possible to make measurements of the SO_2 concentration.

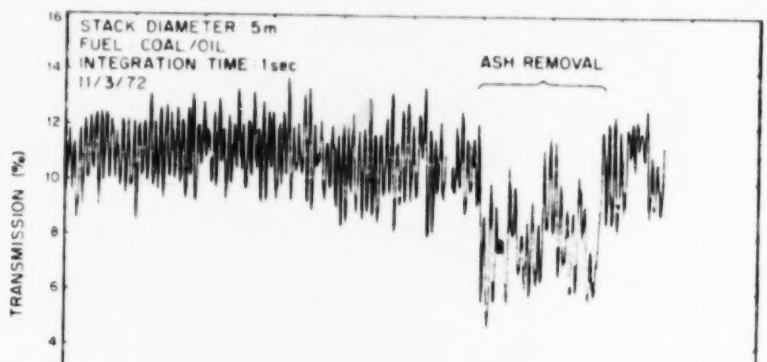

Fig. 23. Transmission of diode laser radiation across 5-meter-wide coal-burning stack in Worcester, Massachusetts (Webster Street Generating Station).

In Fig. 23, transmission of the laser beam is shown for the operating stack over a 1.5-hour period. The 45-second oscillations are real, as they also showed up at times on the point-sampled data, but their origin is unknown. They could be caused by fluctuations in the coal feed rate, or resonances between the two exhaust fans. During removal of ashes, the particulate concentration increased abruptly, as indicated by a drop in transmission at 3:25 p.m. (15:25).

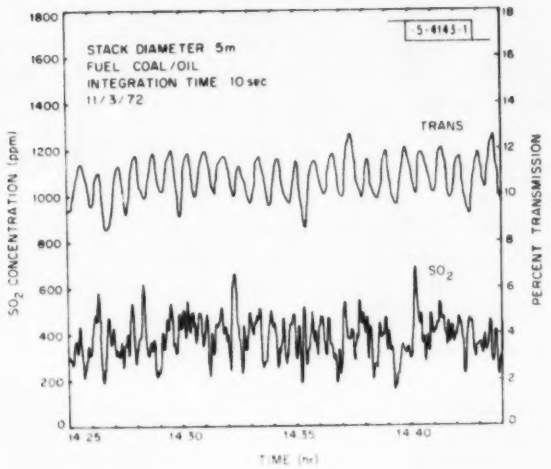

Fig. 24. Transmission and SO_2 measurements at Webster Street Generating Station using diode laser monitoring system. A one-way path was used because of the high attenuation due to particulates.

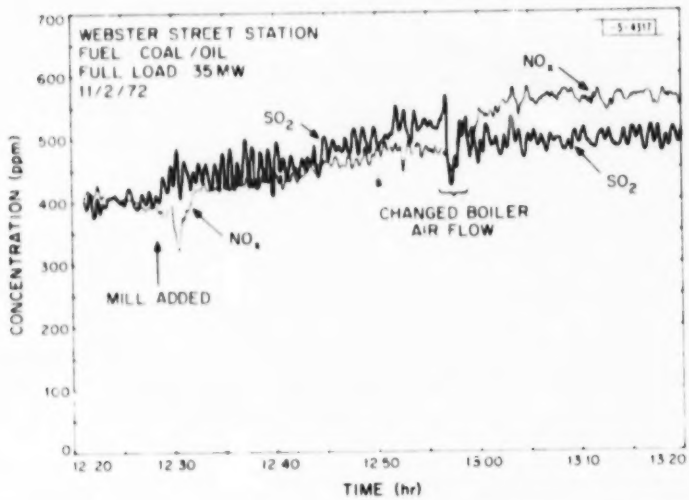

Fig. 25. Measurements of SO_2 and total NO_x at Webster Street facility using a Dynascience sampling monitor.

At times, the SO_2 reading also exhibited oscillations having a periodicity of 45 seconds, but such oscillatory behavior was not usually present. Figure 24 shows transmission and SO_2 values over a 19-minute period. In each case the integration time constant is 10 seconds. The mean SO_2 value is around 400 ppm, with excursions between 200 and 600 ppm.

Using the Dynascience sampler, the SO_2 concentration was found to vary between 400 and 500 ppm. This range was found to hold from day to day, and was relatively constant even when the power load was reduced from 35 MW to 18 MW. (A lower NO_x value was measured during reduction of the load, as expected.) Results of on-line sampling of the SO_2 and NO_x content of this stack during the day preceding the diode laser measurements are shown in Fig. 25. This particular time interval was selected to show that the 45-second oscillations which were detectable in transmission across the stack can show up in the SO_2 measurement as well. As mentioned earlier, however, such oscillations in the SO_2 content are not usually present.

Because of a scheduling conflict, no simultaneous measurements involving both monitoring techniques were carried out. Nevertheless, some conclusions can be drawn on the basis of these measurements.

(1) Periodic (45-second) oscillations in the transmission of the laser beam across the stack appeared, at times, in the SO_2 readings of the Dynascience point-sampling monitor. Is the point sampler responding to fluctuations in the particulate concentrations?

(2) The average concentration of SO_2 in the stack gas, as determined by the diode laser technique, was approximately 50 ppm below that measured by the Dynascience sampler. Does this reveal a fundamental operating difference between the two methods (e.g., free SO_2 molecules vs those absorbed on particles), or does it indicate the difference between sampling at one point in the stream and obtaining an average value across the stream?

Experiments directed toward answering the questions raised by these measurements can be performed under laboratory conditions. The conclusions can have an important bearing on the future course of source-monitoring instrumentation.

7. RECOMMENDATIONS FOR FUTURE STUDIES

With the system now operational, we recommend that several studies be performed in the laboratory before its application in the field. These are described as follows.

7.1 Temperature Dependence

Although the region for SO_2 detection was selected by virtue of its relatively temperature-independent absorption coefficient, the temperatures within a stack can fluctuate so strongly that the system response should be checked as a function of SO_2 gas temperature. The test is relatively simple, and would yield valuable information with regard to the analysis of any in situ data.

7.2 Interferences from Other Gases

As shown in Section 5.4, interferences due to NH_3 and C_2H_4 can occur at certain wavelengths. NO and CO are also present in large quantity, but they should not interfere because of a lack of spectral lines beyond approximately 5 microns. However, a study should be made of other gases

which may be present to see if their wavelengths for absorption are near those for the diodes of the present system; if there are some, an interference measurement should be made.

7.3 Laser Tuning and Directionality

There is evidence that some of the diode lasers undergo a change in the direction of emission when the "tuned" pulse is triggered. When this is the case, interpretation of the data can be difficult. It is possible, however, to overcome this problem by initially setting up the system with the tuning pulse set equal to zero. With the "zero" retroreflector and across-the-stack retroreflector identically aligned, the presence of the tuning pulse will shift the direction such that it can be monitored on the "zero" retroreflector, for which the "zero" control is then adjusted to produce a reading of 0 ppm. By sliding the "zero" retroreflector out of the way, the across-the-stack transmission will yield directly the ppm SO_2 in the stack.

The cause of the above directionality is not understood at the present time, although new fabrication techniques, such as the use of stripe-geometry contacts, are expected to improve the characteristics. For very sensitive applications, two different lasers can be used to produce the electromagnetic energy simultaneously at two wavelengths for ratio analysis.

ACKNOWLEDGMENTS

We acknowledge the generous cooperation of personnel at Hanscom Field in Bedford, Massachusetts in permitting several preliminary measurements to be made at the base heating plant facility; and of officials of the Massachusetts Electric Company for assistance in the final system measurements at their coal-burning power plant in Worcester.

Appreciation is also expressed to Charles E. Rodes of the Stationary Source Emissions Measurement Methods Branch of the Environmental Protection Agency, for performing correlative point-sampling measurements at the Worcester power plant, and for assisting in the data analysis.

REFERENCES

1. For a general review, including extensive references, see Tunable Infrared Lasers and Their Applications to Air Pollution Measurements, E. D. Hinkley, J. Opto-Electronics 4, 69 (1972); also included as Appendix B of this report.

2. Laser-Raman Radar, H. Inaba and T. Kobayasi, ibid. 4, 101 (1972); Mie Scattering Techniques for Air Pollution Measurement with Lasers, R. T. H. Collis and E. E. Uthe, ibid. 4, 87 (1972); Laser Raman Radar Detection Based on a Sampling Technique, L. R. Lidhold, ibid. 4, 133 (1972); A Study of Tunable Laser Techniques for Remote Mapping of Specific Gaseous Constituents of the Atmosphere, Raymond M. Measures and Gilles Pilon, ibid. 4, 141 (1972).

3. Development and Application of Tunable Diode Lasers to the Detection and Quantitative Evaluation of Pollutant Gases, Final Technical Report prepared for the Environmental Protection Agency under Electronic Systems Division Contract F19628-70-C-0230 by M.I.T., Lincoln Laboratory, 30 September 1971.

4. Crystal Growth, Annealing, and Diffusion of Lead-Tin Chalcogenides, A. R. Calawa, T. C. Harman, M. Finn, and P. Youtz, Trans. Met. Soc. Amer. Inst. Mining Eng. 242, 374 (1968).

5. Tunable-Laser Spectroscopy of the ν_1 Band of SO_2, E. D. Hinkley, A. R. Calawa, P. L. Kelley, and S. A. Clough, J. Appl. Phys. 43, 3222 (1972).

6. We are indebted to S. A. Clough of the Air Force Cambridge Research Laboratories for making his computer line listing for SO_2 available to us.

APPENDIX A
OPERATING AND CIRCUIT DETAILS

This Appendix contains operating details and a description of the electronic components of the Diode Laser Monitoring System. It is divided into four main sections:

I. Operating Procedure
II. Electronic Circuits and Timing Sequence
III. Electronic Alignment Procedure
IV. Cryogenic Dewar Preparation

I. OPERATING PROCEDURE

Figure A-1 shows the front panel of the electronics control console. Figure A-2 is a top view of this cabinet with the cover removed. The system is made operational (except for the diode laser power) by placing the main power toggle switch of Fig. A-1 in the "on" position. A

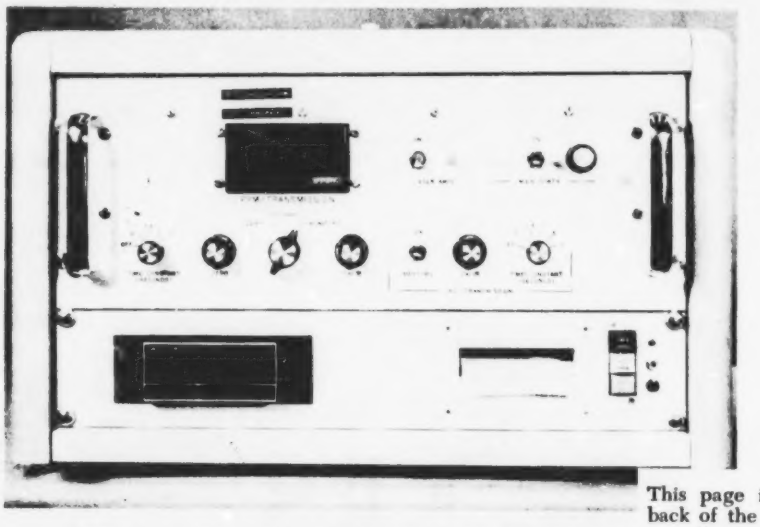

Fig. A-1. Front view of electronics control console.

This page is reproduced at the back of the report by a different reproduction method to provide better detail.

yellow light to the left of this switch indicates the application of main power, and the fuse to the right will light if it has blown. As soon as the main power has been turned on, the "Laser Ampl" toggle switch can be raised to energize the power supply to the laser drive circuit. Because there can be damaging currents supplied to the diode laser if the main power is turned on or off while the "Laser Ampl" switch is "on," a time-delay relay is incorporated. This relay, designated as K1 in Fig. A-2, shorts out the diode laser for a period of 10 seconds after the main power is applied, allowing time for power-supply-induced transients to disappear. In the event of a power failure to the entire system, the relay will also protect the diode.

Figure A-3 is a close-up view of the optics table. Initial alignment of the beam-splitter, calibration cell, and infrared detector should be performed in the laboratory so that no further adjustment is necessary at the field site. Optical alignment in the field then requires the rotation

Preceding page blank

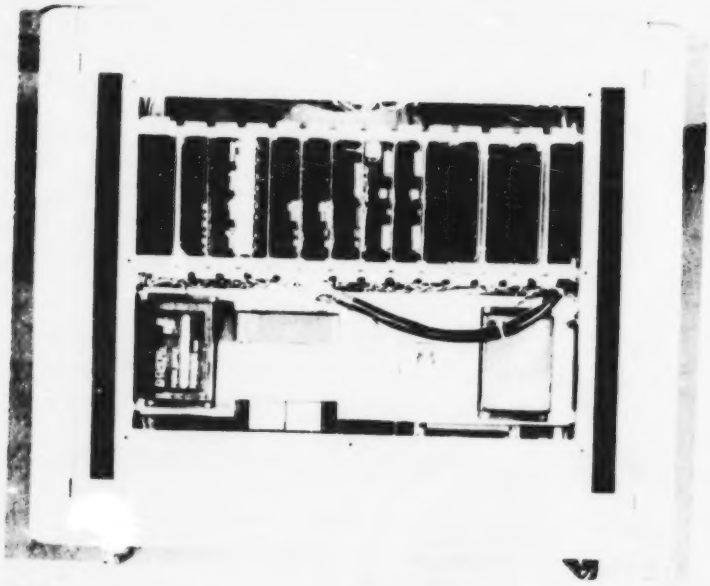

Fig. A-2. Top view of electronics control console, with cover open to show circuit board configuration.

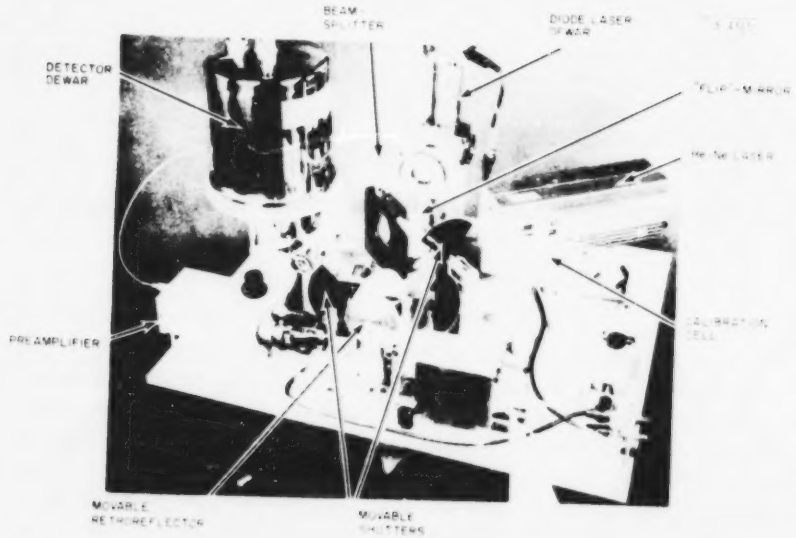

Fig. A-3. Detailed view of optics table, illustrating various components.

This page is reproduced at the back of the report by a different reproduction method to provide better detail.

of the laser Dewar for maximum transmission signal in both the "zero" and "calibrate" positions of the front panel selector switch, followed by an orientation of the entire assembly for maximum transmission across the stack to the retroreflector, and back. The optical and electrical adjustments are as follows.

(1) Set instrument panel function switch alternately to "zero" and to "calibrate," rotating laser Dewar until both transmission signals, as indicated by the analog recorder, are the same as those achieved previously in the laboratory. This ensures that the laser Dewar is oriented properly. (Since the detector Dewar cannot be moved, no adjustment of its collecting lens is warranted.)

(2) Position the retroreflector on the opposite side of the stack. Set function switch to "monitor," and with the aid of the visible helium-neon laser (previously aligned collinearly with the diode laser beam), orient the assembly until the laser beam hits the retroreflector. With the He-Ne laser "flip" mirror removed, correct for any slight alignment difference by a small rotation or tilt of the table for maximum "transmission" signal. The system is now aligned optically.

(3) Return function switch to "zero." This causes the movable retroreflector to intercept the beam before it can enter the stack. By adjusting the "zero" control knob, set the SO_2 analog recorder pen to zero volts. The digital panel meter will also read zero if the panel toggle switch is down (in the "monitor" position). Both the tuned and untuned laser pulses now produce equal detector output in the absence of any SO_2.

(4) Set function switch to "calibrate," thereby directing the laser beam through the 10-cm-long (calibration) cell containing a known quantity of SO_2. The ratio of calibration cell length to smokestack diameter is multiplied by the gas concentration in the cell to yield a value for the comparable SO_2 concentration in the stack. For example, if the calibration cell contains 20,000 ppm SO_2, the equivalent concentration for a smokestack 10 meters in diameter is $0.1/10 \times 20{,}000 = 200$ ppm. The monitor "calibrate" control knob would then be adjusted so that the digital panel meter reads 0200.

(5) Set function switch to "monitor," and select appropriate time constants for "SO_2" and "transmission" readings between 0.1 and 10 seconds. The system is now operational.

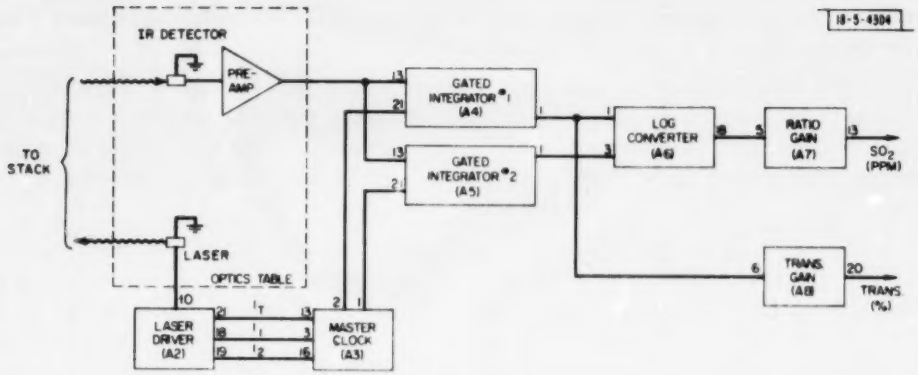

Fig. A-4. Block diagram of electronic modules for diode laser stack-monitoring system.

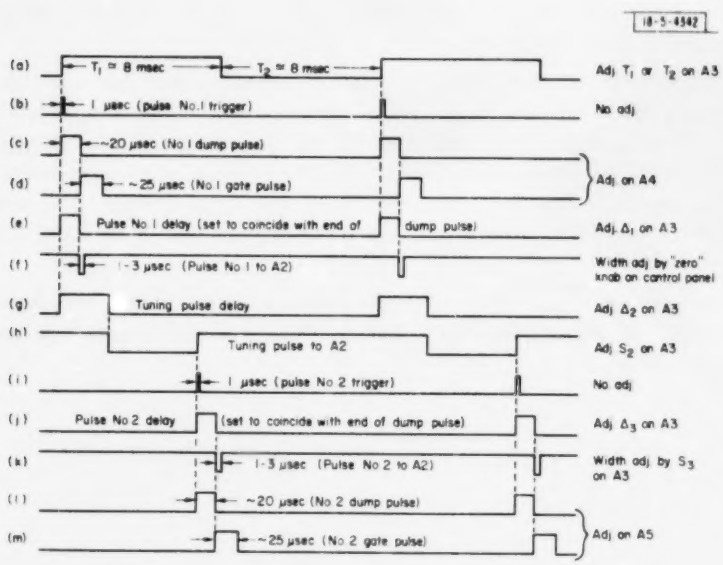
18-5-4342
(a) $T_1 \simeq 8$ msec
$T_2 \simeq 8$ msec
Adj T_1 or T_2 on A3
(b) 1 μsec (pulse No.1 trigger)
No adj
(c) ~20 μsec (No 1 dump pulse)
(d) ~25 μsec (No 1 gate pulse)
Adj on A4
(e) Pulse No 1 delay (set to coincide with end of dump pulse)
Adj Δ_1 on A3
(f) 1-3 μsec (Pulse No 1 to A2)
Width adj by "zero" knob on control panel
(g) Tuning pulse delay
Adj Δ_2 on A3
(h) Tuning pulse to A2
Adj S_2 on A3
(i) 1 μsec (pulse No 2 trigger)
No adj
(j) Pulse No 2 delay (set to coincide with end of dump pulse)
Adj Δ_3 on A3
(k) 1-3 μsec (Pulse No 2 to A2)
Width adj by S_3 on A3
(l) ~20 μsec (No 2 dump pulse)
(m) ~25 μsec (No 2 gate pulse)
Adj on A5

Fig. A-5. System timing sequence, indicating locations for making adjustments. All pulses are 3-5 volts in amplitude.

II. ELECTRONIC CIRCUITS AND TIMING SEQUENCE

The block diagram of Fig. A-4 shows interconnection of the various electronic modular components, each of which is contained on a circuit board within the main console and can be seen in Fig. A-2. (The Preamp is located in a shielded box on the optics table near the detector.) The timing sequence is depicted in Fig. A-5 with individual pulses denoted by (a) through (m).

The Master Clock (A3) contains an oscillator (a) that feeds the logic generating circuits. These circuits control the Laser Driver (A2), which cause the diode laser to emit pulses of infrared energy alternately "on" and "off" an SO_2 absorption line. A short pulse I_1 is fed into the laser at a time determined by (e), with a width determined by (f), causing it to emit at a certain wavelength fixed by the laser crystal composition, its length, and the ambient temperature. The laser is then heated slightly with a relatively long "tuning" pulse, I_t, of duration determined by (g) and (h), and of adjustable amplitude (to 500 mA) usually below threshold for laser emission. The heating effect shifts the laser emission, λ_1, to another wavelength, λ_2. Radiation at λ_2 is emitted when the laser is driven by a second short pulse, I_2, whose location and width are determined by (j) and (k).

Prior to the current pulse, I_1, Gated Integrator 1 (A4) receives a trigger pulse (b) which causes it to "dump" its old signal in an interval (c) and prepare to receive new information during a gate time set by (d). This information is held until a new cycle of operation is started. At the end of the tuning pulse I_t, a trigger (i) of duration (l) is sent to Gated Integrator 2 (A5) for the "dump" process. The gate to Integrator 2 is turned on by (m), during which time the signal from the preamplifier is stored. If there is SO_2 gas between the laser and detector, the amplitude of the transmitted signals at the "untuned" and "tuned" wavelengths will be different, causing the two integrators to store different voltage levels.

Each of the integrators is an input to the Log Converter (A6) whose output is proportional to the logarithm of the ratio of the two input voltages, V_1 and V_2, such that

$$V_{out} = \log (V_2/V_1), \text{ in volts} \quad .$$

In the event that the untuned pulse is in a region of small absorption compared to that of the tuned pulse, a miniature toggle switch on the Log Converter card (A6) may be switched to the opposite position, so that the output remains positive.

From the Log Converter the steady state signal is processed by the Ratio Gain circuit (A7), which is capable of changing the output voltage to correspond to a particular reading on the 10-volt-full-scale digital panel meter. For example, if 200 ppm SO_2 is used for calibration, the variable gain control of A7 is adjusted for a reading of 0200 on the meter, or 0.2 volt. The Ratio Gain circuit also provides for filtering of noise, with adjustable time constants from under 0.1 second to 10 seconds.

The Transmission Gain circuit receives the larger (in absolute value) of the two inputs to the Log Converter, and processes it in a manner similar to that of the Ratio Gain circuit. For example, if the percent transmission is to be set at 100, then the gain control is adjusted for a panel meter reading (with the toggle switch set to "transmission") of 0100, or 0.1 volt.

The infrared detector is Ge:Cu, of dimensions 3 mm × 2 mm × 2 mm. It is attached to the "cold finger" of a liquid helium Dewar according to the schematic of Fig. A-6, and has a resistance of approximately 100 kilohms when cooled. Optical baffling is provided by 2-mm and 5-mm diameter apertures which restrict the field of view to 30° (f/1.9). The infrared filter, from

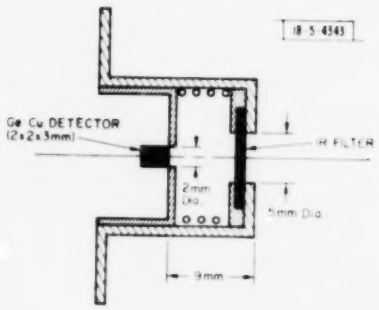

Fig. A-6. Cross section of infrared detector and filter assembly.

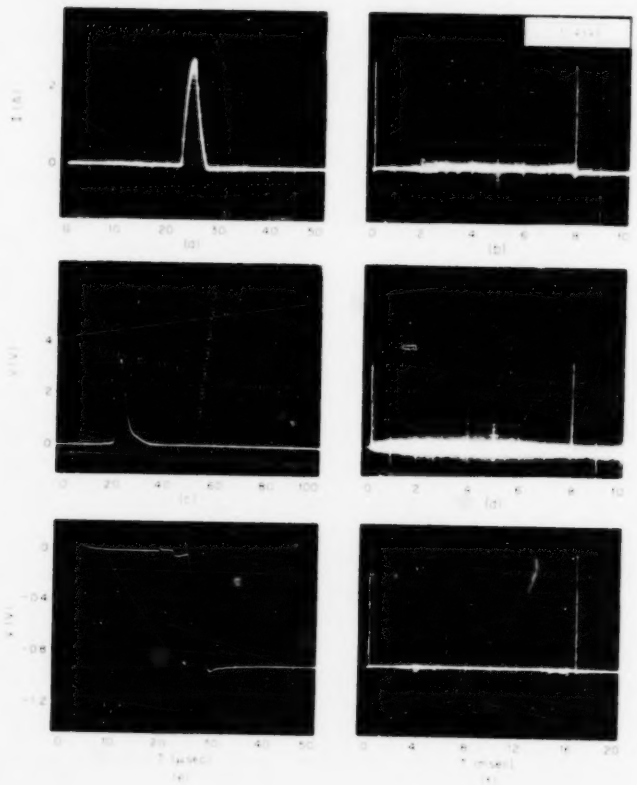

Fig. A-7. Oscillograms of important voltages and currents of the monitoring system. (a) and (b) show the laser current pulses; (c) and (d) the preamplifier signal; and (e) and (f) the output from one of the gated integrators.

Optical Coating Laboratory, Inc., permits radiation only between 1100 and 1227 cm^{-1} to reach the detector. A room-temperature BaF_2 window serves as the entrance port to the detector. In order to reduce the capacitive loading, as well as noise, the preamplifier shown in Figs. A-3 and A-4 is located very near the detector Dewar, so that the lead length is less than 20 cm.

The preamplifier is a low-noise circuit (detector-noise-limited) with a gain adjustable from 5X to 30X by an attached potentiometer. The unit saturates when the output pulse reaches 4.0 volts amplitude and provision has been made to ensure that the preamplifier is within its operating range. This is performed by a measurement of the output voltage from the Transmission Gain circuit under the condition of minimum gain (i.e., with the "Net Transmission – Calib." knob fully counterclockwise). As long as the output of the preamplifier is less than 4 volts, the voltage recorded by the "transmission" pen of the analog recorder, or that indicated on the digital panel meter (for net transmission) will be less than 0.1 volt. If the final voltage is greater than 0.1 volt, the preamplifier gain should be reduced. If a further reduction in signal is still necessary, then a smaller laser current amplitude or width can be used.

Typical oscillograms of voltage and current waveforms under operating conditions are shown in Fig. A-7. In (a) is shown the laser current pulse 1 of 2 amperes, with a full width at half-maximum of 3 μsec. In (b) the time scale is compressed to illustrate the entire sequence of currents applied to the diode laser: pulses 1 and 2 of nearly equal magnitude and width, and the tuning pulse I_t which extends from 3 to 8 msec, and tunes the laser so that the wavelength emitted at pulse 2 is shifted from that of pulse 1. For 8 msec after pulse 2 there is no current applied to the laser, during which time the junction temperature reverts to its original value before pulse 1 is again applied. A 3.4-volt signal from the preamplifier is shown in (c); and in (d) the preamplifier outputs due to both pulses are shown in the same time scale as (b). The gated integrator is normally at zero volts, as indicated in (e) for time before 24 μsec; but beyond this point the integrator responds to the preamplifier signal, reaching a value of −0.9 volt, and holding this value until the dump pulse occurs, as shown in (f). Integrators 1 and 2 are identical in operation, except for their being gated to pulses 1 and 2, respectively. Their output voltages are negative and serve as comparative inputs to the logarithmic converter, whose output is positive and constant for steady-state conditions. The output from the logarithmic converter is further amplified by the Ratio Gain circuit, which also permits post-detection filtering, and displayed on the analog recorder and digital panel meter as "SO_2 concentration." The larger (in absolute value) of the two outputs from the gated integrators goes to the Transmission Gain circuit as the "transmission" signal, which is displayed in the same manner as the ratio signal.

The current-voltage characteristics of the diode lasers at liquid helium temperature are shown in Fig. A-8. (At room temperature there is no strong rectification because of the narrow energy gap of the semiconductor material.) In cases where degradation of the electrical contact of a laser is suspected to have occurred, new curve-tracer scans should be compared with these. However, in no case should an ohmmeter be used to check for rectification because the standard internal 1.5-volt battery will cause the diode junction region to "break down," resulting in permanent damage to the laser.

Each of the circuits described above is shown in detail in Figs. A-9 to A-15, which constitute the remainder of Section II of Appendix A.

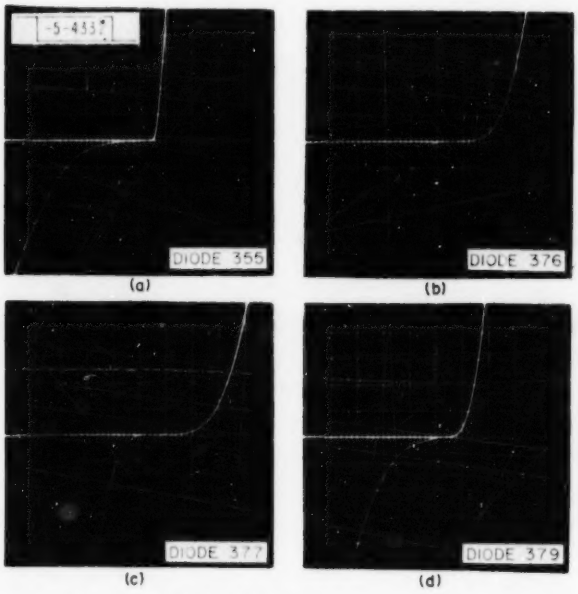

Fig. A-8. Current-voltage characteristics of the system diode lasers at liquid helium temperature. Horizontal scale: 0.2 V/div; vertical scale: 50 mA/div and 0.05 mA/div (for the expanded reverse traces). Voltages and currents are zero at the center of each oscillogram.

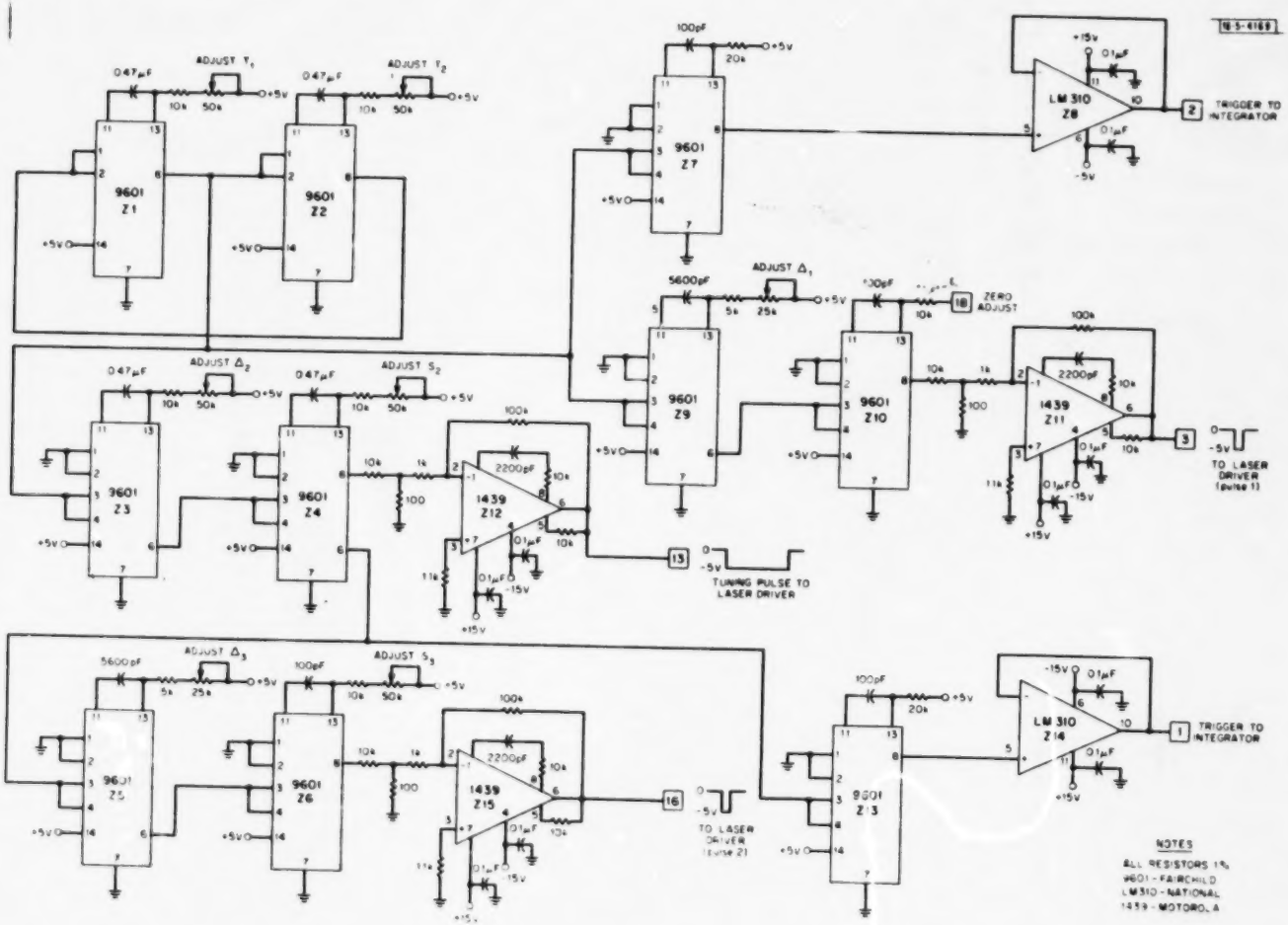

Fig. A-9. Master Clock (A3).

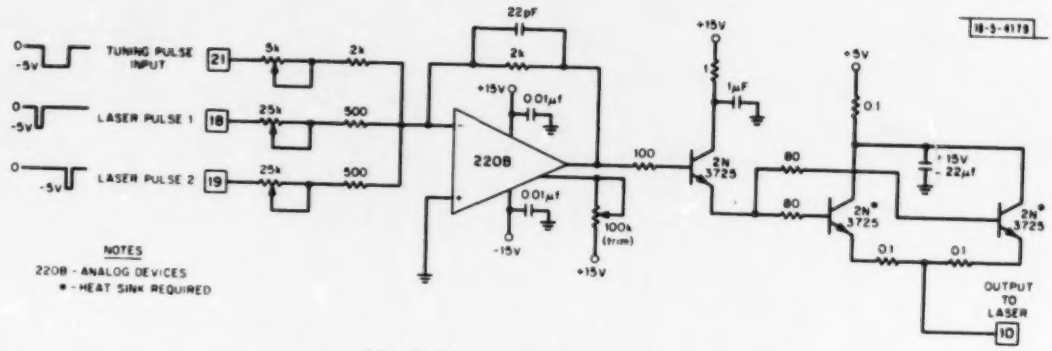

Fig. A-10. Laser Driver (A2).

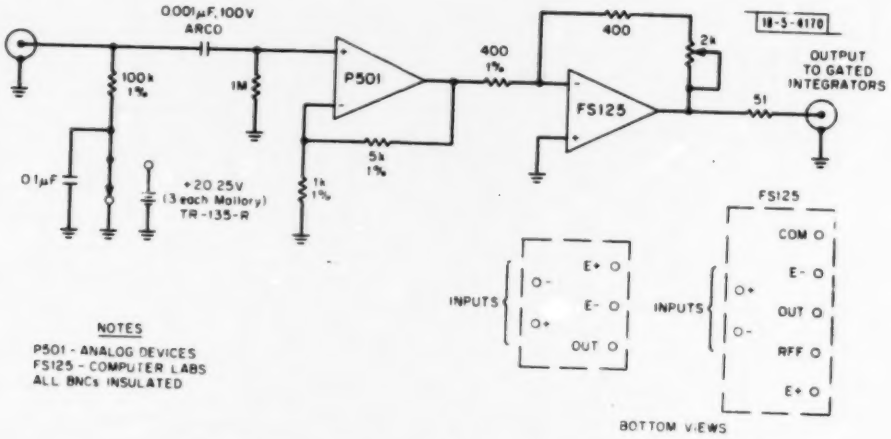

Fig. A-11. Detector Bias Supply and Preamplifier.

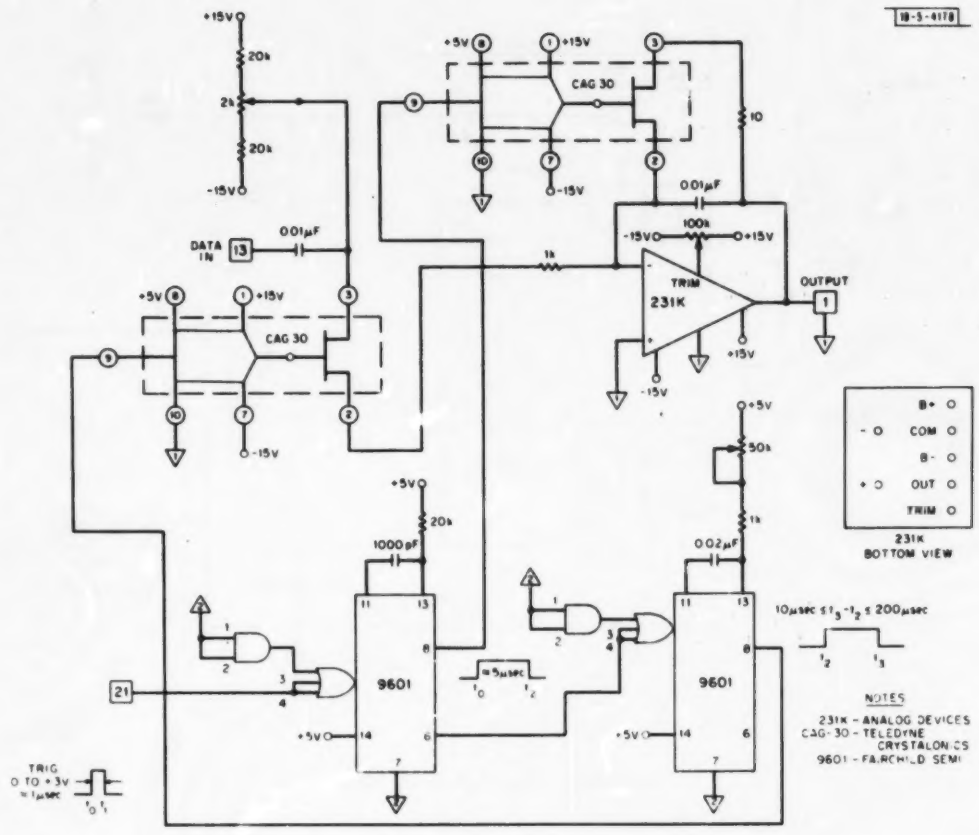

Fig. A-12. Gated Integrator (A4, A5).

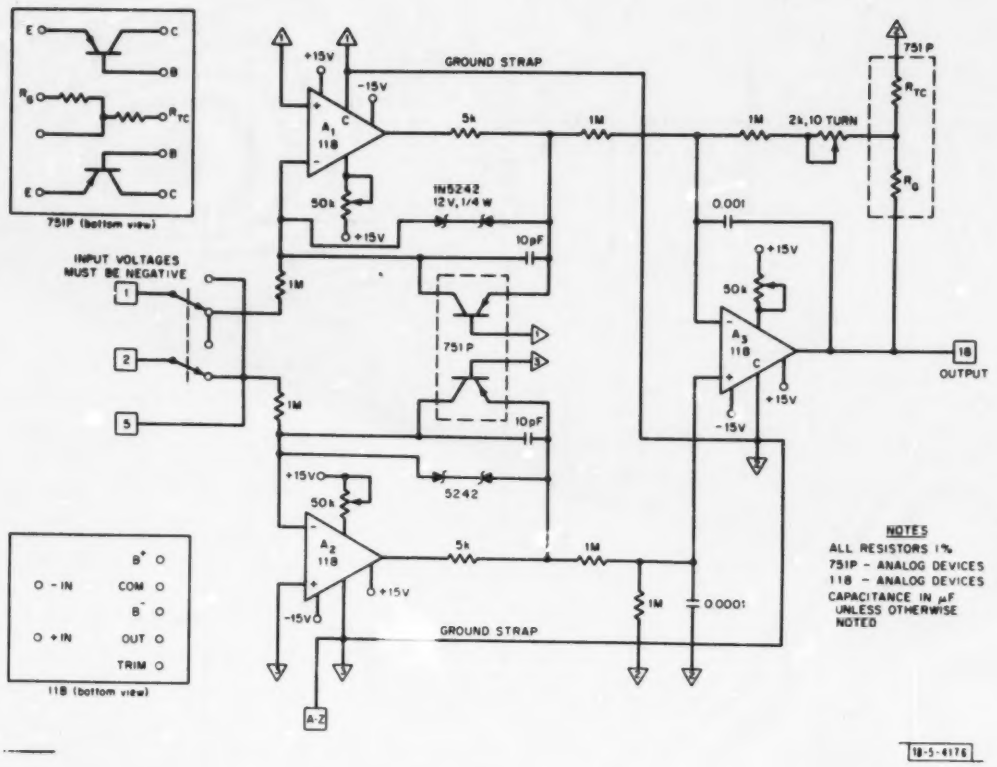

Fig. A-13. Log Converter (A6).

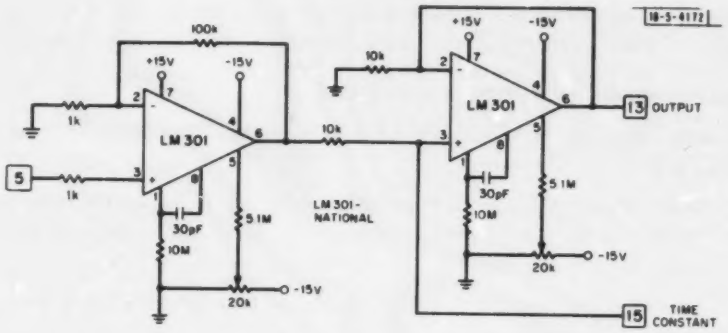

Fig. A-14. Ratio Gain Control circuit (A7).

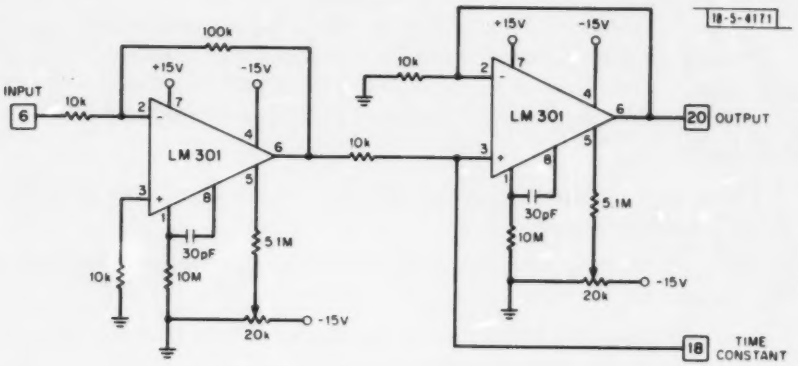

Fig. A-15. Transmission Gain Control circuit (A8).

III. ELECTRONIC ALIGNMENT PROCEDURE

Section III is separated into three parts, each describing a particular aspect of the electronic alignment procedure. Part A details the adjustments to be made immediately prior to monitoring. In Part B are shown adjustments which affect the timing and sequencing of circuits, but are not usually adjusted. Part C concentrates on trim controls for the operational amplifiers.

A. Adjustments for Initial Setup and Monitoring

Several adjustments for the laser current pulses, preamplifier gain, and output signal level are described below.

(1) Laser Driver A2: Tuning Current Amplitude I_t is set for the most optimum value for each laser (i.e., maximum absorption coefficient for SO_2); it should usually be under 100 MA to minimize LHe boil-off.

The other two adjustment potentiometers at the top of the Laser Driver card are for I_1 and I_2, which are usually kept at their maximum values of 2 amperes.

(2) Master Clock A3: The only adjustment which should ever need to be made on this card is S_3, which controls the width of current pulse 2. Only if the signal due to the pulse saturates the detector preamplifier should the width be reduced. The width of pulse 1 is controlled by "zero" knob on the front panel and is adjusted such that the signals due to both pulses are equal in the absence of SO_2.

(3) Preamplifier Gain Control: On the preamplifier is a variable-gain control. It should be set at a maximum (fully clockwise) except when its output approaches 4 volts, where saturation occurs. In order to ensure that the preamplifier output is under 4 volts in the field, where an oscilloscope may not be available, the transmission signal, as measured by the panel DVM, should read less than 0.100 volt with the transmission gain knob (on front panel) at its minimum value (fully CCW).

(4) Panel Controls

(a) "Zero" adjusts width of current pulse 1 so that signals due to 1 and 2 are equal in absence of SO_2.

(b) "SO_2 Calibration" knob adjusts final ratio amplifier gain (circuit A7) to read ppm SO_2 directly.

(c) "Transmission Calibration" knob adjusts final transmission gain (circuit A8) to read directly in percent transmission.

(d) "Time Constants" for SO_2 and transmission readings are independently adjustable on front panel.

(5) Polarity Switch

On the "Logarithmic Converter" Card (A6) is a miniature toggle switch which reverses the two input voltages to this circuit, so that the output voltage remains positive. The position of this switch depends upon the initial wavelength of the diode laser (whether it is in a peak or valley of the SO_2 spectrum), which may vary from one laser to another.

B. Potentiometers Not to Be Adjusted

The following labeled potentiometers do not ordinarily need adjustment, as they control the timing sequence and some noncritical parameters:

(1) On Laser Driver A2, current amplitudes I_1 and I_2 are set at maximum values of 2A. Fine adjustment of current amplitude is difficult, so the laser pulse width controls are normally used to adjust detector output signal.

(2) On Master Clock A3, the basic timing sequence is determined by T_1 and T_2, and the delays for pulse 1, 2, and I_t by Δ_1, Δ_3, and Δ_2, respectively. These should not be adjusted, nor should the width of I_T, governed by potentiometer S_2.

(3) On the two Gated Integrator circuits, A4 and A5, there are two potentiometers marked "B" and "T," which do not normally need adjustment. "B" can be used to set the output voltage to zero in the absence of any input signal, and "T" adjusts the time during which the integrator is "on." It is important that the outputs of A4 and A5 are equal if the inputs are the same; and the adjustment "T" can be used to accomplish this.

C. Operational Amplifier Trim Adjustments

Sixteen operational amplifiers are employed in the system on the various functional circuit boards as well as in the detector preamplifier. Each OP-AMP has been adjusted by an attached potentiometer so that the output voltage is zero when the voltage to its input resistor is zero. Since this trim adjustment has already been made, it should not need to be rechecked unless an OP-AMP is replaced.

IV. CRYOGENIC DEWAR PREPARATION

This section describes evacuation and cool-down procedures for both the laser Dewar and the detector Dewar. The laser Dewar requires liquid nitrogen (LN) in its outer jacket, with liquid helium (LHe) in the center, whereas the Dewar housing the infrared detector requires only LHe.

A. Laser Dewar (Supairco)

Should be pumped to approximately 3×10^{-6} Torr just prior to filling with LN and LHe, according to procedure (1) or (2) below. If evacuation is not possible (e.g., at field site), procedure (2) must be used to permit LHe cryopumping to take place during LN transfer.

Cooling Procedures:

(1) Pre-Cooled (requires 4-5 liters of LHe)

Connect rubber hose between LN tank and inlet (larger diameter) to external jacket. Connect a rubber tube from the outlet (smaller diameter) to center section of Dewar. Keep safety pressure relief disk and Dewar valve warm by using a heat gun. Fill until LN spills from inner section. Connect split hose to outer jacket, and stopper inner section. After 15 minutes, use gaseous He to force LN from inner section. Purge LHe transfer tube with He gas, and immediately fill inner section of laser Dewar, using approximately 4 psi helium gas pressure. LHe fill takes approximately 4 minutes and is noted by a marked increase in size of the water vapor vent cloud.

(2) Direct LHe Fill (requires 6-7 liters of LHe)

Connect rubber hose from LN tank to inlet (larger diameter) of external jacket, leaving outlet (smaller diameter) venting to atmosphere. Keep inner section purged with a small flow of helium gas to prevent condensation. Transfer LN to outer jacket for a few minutes to allow some pre-cooling of the Dewar. If the outside of the Dewar becomes cold, or after the outer jacket has been filled, remove helium gas purge tube and transfer LHe. Because of the relatively warm temperature of the Dewar, there will be "puffs" of water vapor visible for several minutes after transfer, as the LHe continues to cool it. The Dewar should be "topped" off with both LHe and LN about one hour later if a test of 4-5 hours is planned.

(3) "Topping Off" Dewar

In order not to blow out all the LHe in the Dewar during this procedure, the transfer tube is first inserted into the LHe storage Dewar, and 2-4 psi of He gas pressure applied until LHe emanates from the other end of the tube, at which point it is inserted into the laser Dewar.

B. Infrared Detector Dewar (Santa Barbara)

This is a LHe-only Dewar, and does not require LN during operation. It should be pumped to approximately 3×10^{-6} Torr every two weeks, but may need more frequent pumping if LN precooling is used. However, because of the small difference in LHe required, direct LHe transfer is usually adequate, simpler, and avoids any chance that LN is still in Dewar before LHe transfer.

Cooling Procedures:

(1) Direct Transfer (requires 3-4 liters of LHe)

Purge LHe transfer tube with He gas and insert into storage and detector Dewars. Apply 2-3 psi He gas and transfer until vapor plume increases noticeably (2-3 minutes). Reduce He gas pressure, remove transfer tube, and fully screw on cap to detector Dewar; then turn cap counterclockwise 1 full turn. Make sure rubber stopper is on securely (this can be held in place with tape).

(2) Pre-cooling (requires 2-3 liters of LHe)

Fill Dewar with LN, replace cap, and allow to sit for 10-15 minutes. Remove cap, invert Dewar, and "shake" out the LN. Transfer LHe immediately according to the procedures described in (1).

C. LHe Transfer Tube (Janis Research Co.)

Should be evacuated to pressures less than 10^{-5} Torr every 2-3 months. This is not critical because of cryopumping of LHe during transfer, but a better vacuum reduces the amount of LHe required.

APPENDIX B
TUNABLE INFRARED LASERS AND THEIR APPLICATIONS TO AIR POLLUTION MEASUREMENTS*

E. D. Hinkley

This paper describes a number of tunable infrared lasers and techniques employing them for the detection and monitoring of gaseous air pollutants. Recent progress in the development of lasers that can be matched to characteristic infrared absorption or emission lines of certain pollutants suggests wide potential application for sensitive, specific monitoring. Examples to be described include highly specific point-sampling, in situ source monitoring, ambient air monitoring, resonance fluorescence, and remote heterodyne detection.

1. INTRODUCTION

The use of fixed-frequency gas lasers for air pollution detection has been suggested and advanced by several workers over the last few years.[1] By selecting appropriate laser transitions which overlap those of the gaseous pollutants, their concentrations can be measured by direct absorption. However, the match is seldom ideal – and for some important pollutant gases, such as SO_2, there appear to be no entirely satisfactory laser lines. Even when overlaps are found, there may be other reasons why a selected gas laser line is not suitable – such as absorption by other components of the normal atmosphere, or coincidence (interference) with spectral lines of other pollutants which may be present.

During the past two years substantial progress has been made in the development of several types of tunable lasers, and systems utilizing these devices are being built for point-sampling and in situ source monitoring. Tunable infrared lasers have also been proposed for ambient air monitoring[2] (both at ground level and in the upper atmosphere) and for single-ended, remote heterodyne detection of emissions from stationary or mobile sources.[3]

A brief survey will be given of the various types of tunable lasers, followed by a discussion of monitoring techniques which can be used. Most of the experimental results represent work performed in our Laboratory using current-tuned semiconductor diode lasers, although work performed by others will also be described, for completeness. Two recently published articles can provide general background information for laser techniques. Kildal and Byer[4] compare in detail laser Raman scattering, resonance fluorescence, and tunable laser absorption techniques. Melngailis[5] covers in more detail the direct absorption techniques and tunable semiconductor lasers.

2. TUNABLE LASERS

Table I lists the types of tunable lasers which are presently available or under development. We consider only primary tunable laser sources, although other wavelengths are possible by mixing radiation from a tunable laser with that from a fixed-frequency laser.[6]

---

*Published in J. Opto-Electronics 4, 69 (1972), as an invited review paper.

TABLE I
TUNABLE LASERS

	Approximate Coverage (μm)	Single-Mode CW Output (W)	Pulsed Output (W)
Organic Dye Lasers	0.34 – 1.2	5×10^{-2}	10^{7}
Parametric Oscillators	0.5 – 3.75	3×10^{-3}	10^{5}
Semiconductor Diode Lasers	0.63 – 34	10^{-3}	10^{2}
Spin-Flip Raman Lasers	5.3 – 6.2 (CO) 9.2 – 14 (CO_2)	1	10^{3}
Bulk Semiconductor Lasers (Optically pumped)	0.32 – 34*	10^{-3}	–
High-Pressure Gas Lasers (Electron-beam-pumped)	4.8 – 8.5*(CO) 9.1 – 11.3*(CO_2)	–	–

*Predicted

2.1 Organic Dye Lasers

Tunable organic dye lasers are available commercially, covering the wavelength range from the near ultraviolet to slightly over 1 μm in the infrared. They operate by optical pumping from the ground state to an excited singlet electronic state of high rotational and vibrational energy.[7] Subsequently the vibration-rotation energy is thermalized by very rapid nonradiative relaxation. A population inversion then exists, and stimulated emission occurs between low vibration-rotation energy levels of the first excited singlet electronic state and higher vibration-rotation levels of the ground electronic state (according to the Franck-Condon principle). Due to the high density of vibration-rotation levels of the large dye molecules and the large widths of these levels in solution, very broad, continuous bands of radiation are emitted (typically several hundred angstroms wide). Narrow-linewidth lasing, tunable within the broad emission band, is achieved by the use of highly frequency-selective optical resonators.

Lasers have been made from dyes of the oxazole, xanthene, anthracene, coumarin, acridine, azine, pthalocyanine and polymethine families. Using various dyes, pulsed operation has been obtained from 0.34 μm to 1.2 μm, with both flash lamps and lasers (notably N_2 and ruby) used as pumps. Linewidths as narrow as 7 MHz have been obtained with an external Fabry-Perot.[8] Peak powers of 10^{7} W, and average powers of the order of 1 W (Ref. 8a) have been observed.

2.2 Optical Parametric Oscillators

Commercial versions of optical parametric oscillators surpass the dye laser in infrared tunability, extending the available range to almost 4 μm. An optical parametric oscillator requires a laser pump source impinging onto a nonlinear crystal. The resulting radiation can be tuned over a wide wavelength range by changing the temperature or orientation of the crystal.[9]

A doubled Nd:YAG-laser-pumped oscillator using $LiNbO_3$ as the nonlinear element can tune from 0.55 to 3.75 μm with a bandwidth of 1 cm^{-1} in the visible and less than 0.25 cm^{-1} in the infrared, with single pulse energy of 1 mJ and repetition rates up to 1000 pps. Using a ruby laser pump source, a spectral region from about 1 μm to 4 μm can be covered with pulse energies

of approximately 0.1 J. The spectral width typically 0.25 cm^{-1} is determined by the crystal length, but it can be reduced by using an intracavity etalon. A bandwidth of 30 MHz (0.001 cm^{-1}) has been recently reported in the vicinity of 2.5 μm for a pulsed $LiNbO_3$ doubled Nd:YAG oscillator using a novel interferometer mode-selector scheme.[10] Recently, parametric oscillation in the 10-μm region has been achieved in the laboratory,[11] indicating that this tunable source can potentially cover all of the important infrared "fingerprint" region between 3 and 15 μm.

2.3 Semiconductor Diode Lasers

Semiconductor diode lasers can be tailored to emit in desired wavelength regions by control of the energy gap – a feature made possible by the development of ternary semiconductor compounds of adjustable chemical composition.[12] The different materials from which semiconductor lasers have been made are shown in Fig. B-1. Complete coverage of the region between 0.63 and 34 μm is now possible. The dashed lines indicate possible future extension of the present limits

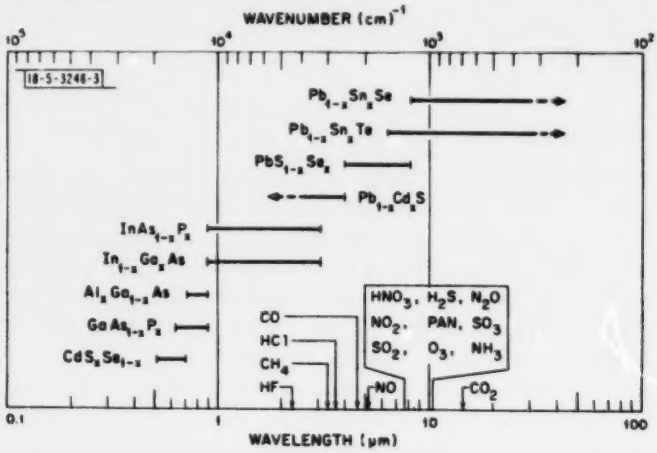

Fig. B-1. Wavelength ranges for semiconductor lasers made from different alloys and compositions. Also shown are some strongly absorbing regions for several common atmospheric pollutants.

(solid lines). Most of the tunable diode laser work has been performed with the lead chalcogenides $Pb_{1-x}Sn_xTe$ (between 6.5 and 34 μm), $PbS_{1-x}Se_x$ (between 4.0 and 8.5 μm), and $Pb_{1-x}Cd_xS$ (between about 2.5 and 4 μm). Principal absorbing wavelengths of some of the important pollutant gases are indicated at the bottom of this figure. It should be noted that with these three semiconducting compounds, nearly all of the important pollutants can be detected.

Figure B-2 shows a semiconductor diode laser in its standard package, which is 1 cm in over-all length. (The entire unit is approximately the size of an average transistor.) The diode crystal is mounted on a copper stud which serves as one electrical contact. A silver ribbon serves as the other contact. Laser emission is produced by passing a current through the diode; this current can be supplied by a small battery or DC power supply for CW operation, or by a pulser for pulsed operation. There are several ways to "tune" a diode laser, the simplest being to change the magnitude of an applied direct bias current, which changes the junction temperature through heating.[13] Since the refractive index within the laser cavity is temperature-dependent,

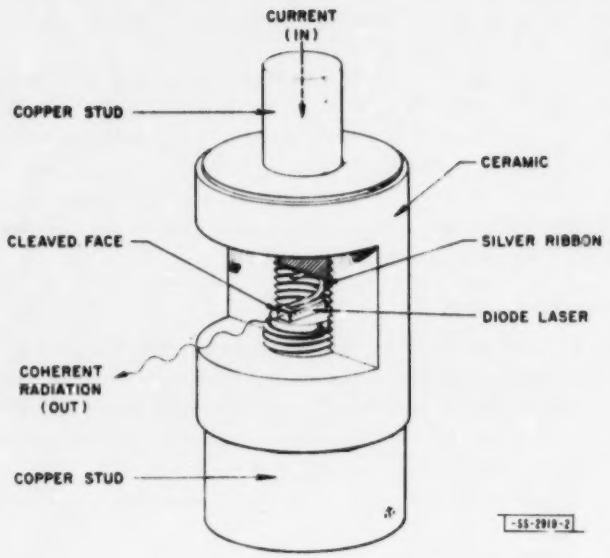

Fig. B-2. Semiconductor diode laser in a standard package having an over-all length of 1 cm. The laser itself has approximate dimensions of 0.12 × 0.05 × 0.03 cm. Tuning is accomplished by changing the direct current applied to the diode.

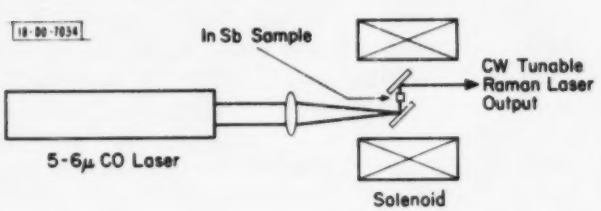

Fig. B-3. Experimental arrangement for a CW spin-flip Raman laser consisting of an InSb semiconductor crystal pumped with a CO gas laser. The magnetic field produced by the solenoid controls the electronic energy levels within the semiconductor, permitting wavelength-tuning.

the laser wavelength changes. Although this type of tuning is thermal, it is still relatively fast because of the limited volume involved. Modulation frequencies of several hundred Hertz can be applied before thermal inertia becomes very noticeable, and useful experiments have been carried out with frequencies as high as 10 kHz.

Current-tuned semiconductor diode lasers have been used to perform Doppler-limited spectroscopy on several gases: SF_6, NH_3, C_2H_4 in the 10-μm region,[14,2], NO, CO, and water vapor around 5 μm (Ref. 15), and an extensive study of the ν_1 band of SO_2 in the 8.7-μm region.[16]

At present, the greatest obstacle to broader application of semiconductor lasers is their requirement for cryogenic cooling. Large improvements in efficiency are expected to relax these cooling requirements to the point where pulsed operation even at wavelengths as long as 10 μm will be possible at temperatures above 100°K.

2.4 Spin-Flip Raman Laser

The spin-flip Raman laser is a device which uses a fixed-frequency laser (at present, a CO or CO_2 gas laser) to pump a semiconductor crystal at cryogenic temperatures and in a magnetic field.[17] The pump laser photons lose energy when they collide with electrons in the crystal and flip their spin. The down-shifted Raman photon is separated in energy from the pump photon by the magnitude of the electron spin energy $g\beta H$, where g is the conduction electron g-factor, β the Bohr magneton, and H the magnetic field strength. Consequently, the output frequency depends on the magnetic field.

A schematic drawing of a spin-flip Raman laser using a CO laser pump and InSb semiconductor is shown in Fig. B-3. A linewidth of 1 kHz for the tunable laser radiation has recently been reported by Patel on the basis of heterodyne measurements.[18] The spin-flip Raman laser has been used to obtain spectroscopic data of NH_3 in the 10-μm region[19] and of NO around 5 μm (Ref. 20).

2.5 Optically Pumped Semiconductor Lasers

A Q-switched Nd:YAG laser has been used to pump samples of the ternary compound semiconductor $In_xGa_{1-x}As$ at room temperature, producing laser radiation at 1.09 and 1.12 μm (Ref. 21). Recently, Melngailis achieved CW laser emission from a liquid-helium-cooled $Pb_{0.88}Sn_{0.12}Te$ crystal pumped with a GaAs diode laser.[21a] It appears that, by using commercially available GaAs diode lasers as pump sources, tunable semiconductor lasers can be made which have some of the advantages of gas lasers, such as high output power and good beam quality, in addition to the relative simplicity, ruggedness, and small size characteristic of diode lasers.

2.6 High-Pressure Gas Laser

At pressures of 10-15 atmospheres, adjacent vibration-rotation lines, which are responsible for emission in gas lasers, overlap such that lasing can occur at intermediate wavelengths as well. At present, electron-beam excitation is required for this potentially powerful tunable source of infrared radiation, and several laboratories are investigating its potential for spectroscopic applications.[22]

3. MONITORING TECHNIQUES

Comparison is often made between tunable laser techniques and those involving conventional infrared instrumentation for air pollution monitoring. The laser system usually has better

sensitivity and specificity because of its higher usable power in a narrow spectral bandwidth, compared with that available from thermal sources. A comparison of resolution is illustrated in Fig. B-4, where a diode laser beam at 10 μm was transmitted through a laboratory-quality grating spectrometer with narrow (80-μm-wide) slits. The smooth bell-shaped curve represents the spectrometer slit function, with a half-width (resolution) of 0.18 cm^{-1}. The narrow absorption lines were produced by introducing 0.5 Torr of ethylene into a 30-cm-long gas cell in front of the spectrometer. These lines are predominantly Doppler-broadened to a width of 66 MHz (0.0022 cm^{-1}). The laser linewidth itself is two or three orders of magnitude narrower than this.[23] It is clear that any attempt to use this spectrometer to evaluate the high-resolution spectra of ethylene will suffer, both in terms of sensitivity and specificity, because of overlap and a severe reduction in intensity produced by the relatively wide spectral interval accepted by the instrument.

For actual in situ measurements, spectral lines of pollutant gases which are this narrow would only occur at very high altitudes – in and above the stratosphere. Nevertheless, even at ground level where atmospheric pressure broadens these ethylene lines to a value of approximately 0.2 cm^{-1}, some instrumental broadening will be produced by even this spectrometer, and substantially more by one which can be used in the field.

Three fundamental monitoring techniques employing tunable lasers are: remote heterodyne detection, resonance fluorescence, and direct absorption. Each has its particular advantages and applications, as described below.

3.1 Remote Heterodyne Detection

This technique represents a completely passive, single-ended laser system for the detection of gaseous pollutants from stationary or mobile sources. Characteristic infrared emission lines from a pollutant gas are detected by heterodyning them with tunable laser radiation of the same wavelength, using the configuration of Fig. B-5. The laser radiation and that from the source are directed onto a wideband infrared detector cooled to liquid helium temperatures. By scanning the laser wavelength through that of the pollutant emission line, a beat frequency is produced whenever the difference frequency between the two infrared signals is within the bandpass of the detector/amplifier system; the amplitude of the signal is related to pollutant concentration. The signal-to-noise ratio is given by[2]

$$\frac{S}{N} = [1 - \exp(-\alpha_c' cL)] \left[\frac{1}{\exp(h\nu/kT_g) - 1} - \frac{\epsilon_b}{\exp(h\nu/kT_b) - 1} \right] [B\tau]^{1/2} \quad , \qquad (1)$$

where α_c' is the absorption coefficient of the line per ppm of gas concentration (c), L is the thickness of the plume, T_g is its temperature, ϵ_b is the emissivity of the background at temperature T_b, ν is the infrared frequency, h is Planck's constant, k is Boltzmann's constant, B the system bandwidth and τ the post-detection integration time. Equation (1) is also based on the following assumptions: (a) that the IF bandwidth is less than the emission linewidth; (b) that the emission and absorption due to the pollutant in the ambient atmosphere is not important because of a low concentration there relative to that in the plume; (c) that the background attenuation from the wings of other molecular absorption lines is negligible; and (d) that the local oscillator has sufficient power to overcome the other sources of noise. Equation (1) holds, regardless of range, as long as the field of view of the collecting telescope is fully subtended by the plume; in the infrared, with collection optics only a few centimeters in diameter, it should be possible to detect pollutants one kilometer away.

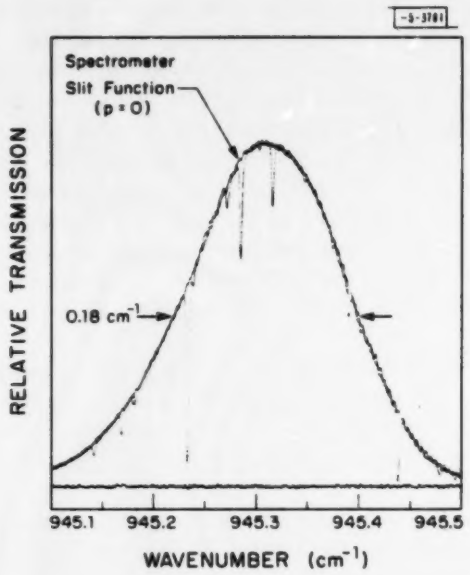

Fig. B-4. Transmission of tunable $Pb_{0.88}Sn_{0.12}Te$ diode laser radiation through a grating spectrometer with 80-μm slits, showing the bell-shaped slit function. The narrow absorption lines are produced when 0.5 Torr of C_2H_4 was introduced into a 30-cm-long cell in front of the spectrometer.

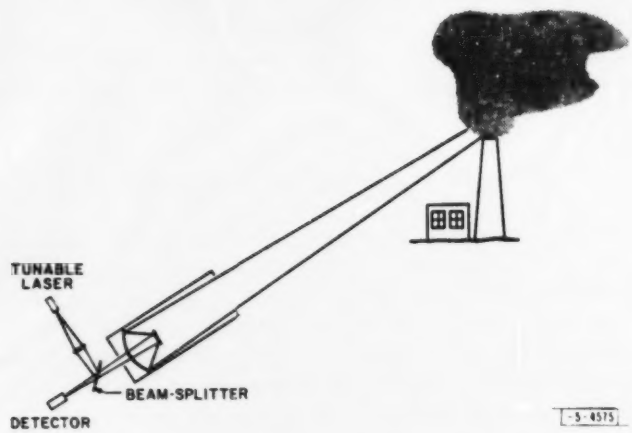

Fig. B-5. Configuration for remote heterodyne detection of pollutant gases from a smokestack using a tunable-diode-laser local oscillator.

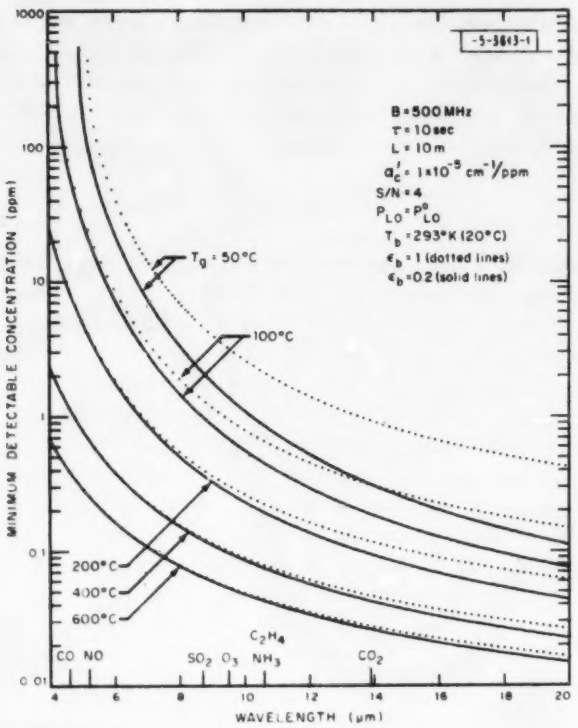

Fig. B-6. Theoretical wavelength dependence for remote heterodyne pollutant monitoring for various gas temperatures, and for background emissivities of 0.2 and 1.0. Useful wavelengths for some pollutant gases are indicated on the abcissa. Other parameters are shown in the figure.

Under these conditions the minimum detectable concentrations for pollutant gases with line strengths of 1×10^{-5} cm^{-1}/ppm are shown in Fig. B-6 as a function of wavelength and for different source temperatures and background emissivities. Concentrations of a few ppm of NO and CO at 400-600°C can be detected, and similar sensitivities are achievable for C_2H_4 and NH_3 (at longer wavelengths) at a temperature of only 50°C. Since SO_2 in the 8.7-μm region has a measured absorption strength almost 10 times smaller, the minimum detectable concentrations for this gas should be raised accordingly.

The local oscillator power necessary to satisfy assumption (d) above is given by the equation[24]

$$P_{LO}^o = \frac{(kT_A)(h\nu)}{\eta e^2 G^2 R_L} \quad , \qquad (2)$$

where T_A is the noise temperature of the amplifier, G the infrared detector gain and η its quantum efficiency, R_L the load resistance, and e the electronic charge. For an amplifier with a noise temperature of 240°K (noise figure of 2.4 dB), and assuming $\eta = 0.5$, $G = 0.12$, $R_L = 50$ ohms, and $\lambda = c/\nu = 10$ μm, we obtain $P_{LO}^o = 12$ mW.

Using state-of-the art infrared detectors and low-noise amplifiers, the local oscillator power of 12 mW is prohibitive, producing not only excessive heating of the detector, but a substantial

liquid helium boil-off. When wideband ($\sim$500 MHz) photodiodes having nearly unit quantum efficiency become available, the local oscillator power requirement will be less than 100 μW – a more realistic value. Experimentally, heterodyne theory has been confirmed by measurements of thermal radiation from a calibrated source; and lines from hot ethylene (600°K) near 10 μm were detected using a CO_2 laser as local oscillator and a Ge:Cu photoconductor as infrared detector.[3]

3.2 Resonance Fluorescence

Absorption of tunable laser light, and detection of subsequent re-radiation, can be used for remote single-ended, detection. Because the laser radiation is directed into the atmosphere, this technique is active, rather than passive. Fluorescence can be excited by pumping either at vibrational frequencies of the molecules, which require lasers at infrared wavelengths, or at electronic transition frequencies, which fall in the visible or ultraviolet part of the spectrum. Several gases, such as SO_2, O_3, NO, NO_2, NH_3, HCOH (formaldehyde), and C_6H_6 (benzene), have absorption bands in the ultraviolet. However, there is a potential problem due to overlap between individual bands, some of which are quite broad. Moreover, atmospheric transparency becomes poor as we approach the vacuum ultraviolet. The electronic transitions should be important for detecting metal vapors such as As, Be, Cu, Zn, Na, and Hg. Atomic sodium has been detected at altitudes of about 90 km, in concentrations of the order of $10^4/cm^3$ using a dye laser tuned to the D lines.[25] For resonance fluorescence in the infrared, Kildal and Byer[4] predict that with a tunable optical parametric oscillator at 4.7 μm, emitting 1 mJ pulses, 100 nsec wide, with a 0.1 cm^{-1} spectral width, it should be possible to detect 2 ppm of CO at a range of 100 meters.

3.3 Absorption

Direct absorption of tunable laser radiation offers the greatest versatility of the three schemes discussed. Point sampling at reduced pressure permits very high specificity as the infrared "signatures" of pollutant gases become observable. Accordingly, this technique can also be used to calibrate other instrumentation used for point-sampling. In situ source monitoring can be performed by transmitting the laser radiation across the effluent stream, leaving the stream itself essentially undisturbed. Transmission of tunable laser radiation over long atmospheric paths can be used to attain the high sensitivity required for ambient-air monitoring.

3.3.1 Point Sampling

In point-sampling applications the total gas pressure can be lowered to reduce or eliminate completely any overlap between adjacent vibration-rotation lines; consequently, very high specificity is possible. One example of this is shown in Fig. B-7, containing tunable $PbS_{0.60}Se_{0.40}$ diode laser scans of NO in the 5.2-μm region.[15] The characteristic Lambda-doubling of the $R(21/2)_{1/2}$ line at 1912.1 cm^{-1} in the upper trace is an unmistakable "signature" for this gas. Recently, Brueck, Johnson, and Mooradian have observed Lambda-doubling of the $R(1/2)_{1/2}$ line of NO at 1881.0 cm^{-1} using a CO-pumped spin-flip Raman laser.[20]

Kreuzer and Patel[20] have used a 50-mW spin-flip Raman laser in conjunction with an opto-acoustic cell (spectrophone) to detect NO in both the ambient air and in samples of automobile exhaust. By using a mechanical chopper to modulate the intensity of the laser beam, acoustic pulses produced in the cell when the laser is tuned to an absorption line can be detected with a

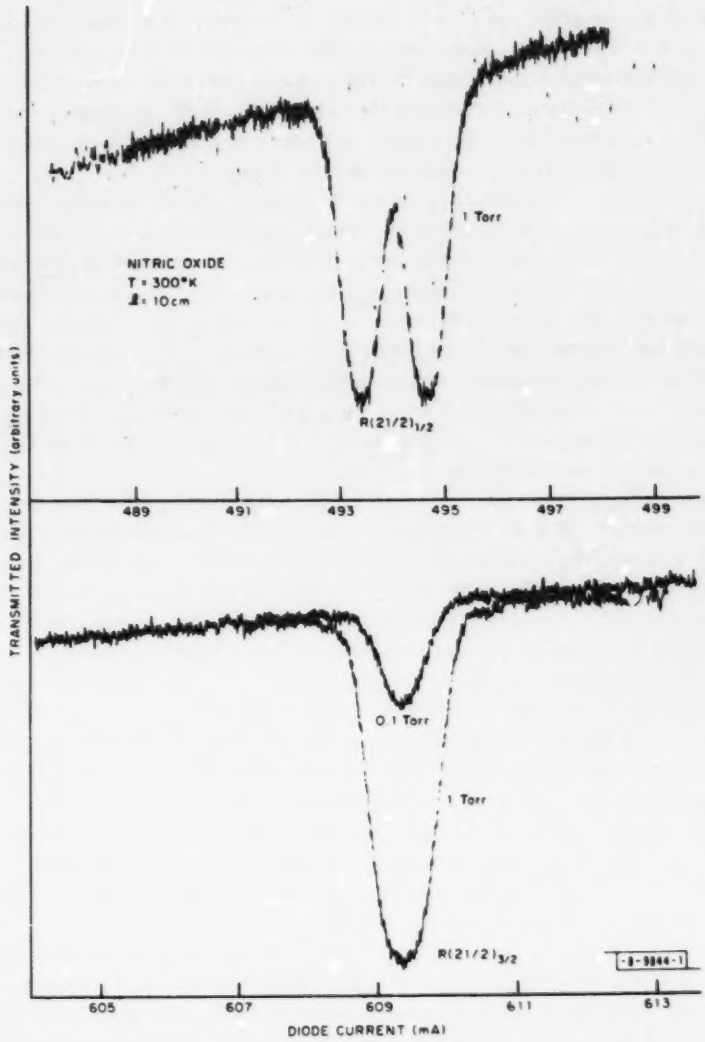

Fig. B-7. Tunable $PbS_{0.60}Se_{0.40}$ diode laser scans of two NO lines in the 1912.1 cm^{-1} region. Lambda-doubling of the $R(21/2)_{1/2}$ line is 300 MHz wide (0.01 cm^{-1}). After Nill, et al.[15]

capacitive microphone, analogous to the operation of a Golay cell. Some of their measurements are shown in Fig. B-8. Trace A is a calibration scan of 20 ppm NO in N_2 at a total pressure of 300 Torr. The lines designated as 1, 5, 6, 8, and 11 are due to NO, while the others represent water vapor. Trace B shows the noise level with the laser radiation blocked, which is primarily Johnson noise in the first amplifier stage.[26] The concentration of NO in a sample of ambient air is estimated to be approximately 0.1 ppm on the basis of Trace C. A sample from a busy road, Trace D, shows a somewhat higher NO content of 2 ppm. In trace E the amount of NO in an exhaust specimen from an automobile is seen to be over 50 ppm.

The spectrophone is useful for detecting absorbed tunable laser radiation because it is sensitive (for tunable lasers with moderate power levels), independent of wavelength, and operates at room temperature. An experiment was performed to compare the absorption signal from a spectrophone with the simultaneously transmitted signal through the cell, monitored with a liquid-helium-cooled Ge:Cu infrared detector. A tunable $Pb_{0.88}Sn_{0.12}Te$ diode laser was used, and the radiation was chopped mechanically before entering the cell. The lower trace of Fig. B-9 is the spectrophone signal proportional to the absorbed laser power p_a; the upper trace represents the infrared detector signal, proportional to transmitted power p_t, where the dashed line corresponds to 100% transmission. The traces are seen to resemble the expected relation to each other, according to the expression $p_t = 1 - p_a$.

By frequency-modulating the laser emission, rather than using amplitude modulation, the signals for transmission and absorption should be identical, except for phase. Derivative detection was used to compare the minimum detectable concentrations of the two techniques. Using a 10-μm $Pb_{0.88}Sn_{0.12}Te$ diode laser having a CW power level of 6 μW, and a 10-cm long cell, the detection limit for C_2H_4 using the spectrophone was a few hundred ppm, whereas that employing the liquid-helium-cooled infrared detector was 1 ppm under the same conditions. The absorption coefficient for the C_2H_4 line was approximately 10^{-6} cm^{-1}/ppm, yeilding a total absorbed power of $P_o\alpha'_c L = 6 \times 10^{-11}$ W, which is close to the noise-equivalent-power of the Ge:Cu infrared detector. Conversely, the Johnson noise limit for the spectrophone imposed by the high-impedance circuitry is approximately 10^{-8} W (Ref. 26), making the spectrophone less appropriate for systems involving tunable laser sources of relatively low power.

Frequency modulation of the laser emission eliminates the need for a mechanical chopper. For a semiconductor diode laser, this is accomplished by superimposing a small (~1 mA) sinusoidal current upon the steady current, and detecting the first derivative at the modulation frequency, or the second derivative at the first harmonic.

Figures B-10 and B-11 illustrate application of this technique to the point-sampling of automobile and smokestack effluents. In Fig. B-10 is a set of first-derivative scans for C_2H_4 near near the Q branch of the ν_7 vibration-rotation band at 10.6 μm. The upper trace represents a 2000-ppm mixture of C_2H_4 in N_2, at a total pressure of 5 Torr, and is used for calibration. The three lower traces were obtained for different samples of raw automobile exhaust, for which the total pressure was also reduced to 5 Torr. The presence of C_2H_4 is unmistakable because of the identical signatures; and by comparing their amplitudes with that of the calibrated sample, a quantitative determination can be made of the C_2H_4 content of each. There is no noticeable interference by any of the other components such as water vapor, CO, NO, and other hydrocarbons, which are also present in large quantities.

Figure B-11 shows results for a similar study of SO_2 in a sample of stack gas from an oil-fired power plant. Using a tunable $Pb_{0.93}Sn_{0.07}Te$ diode laser in the 8.7-μm region of the ν_1 band,

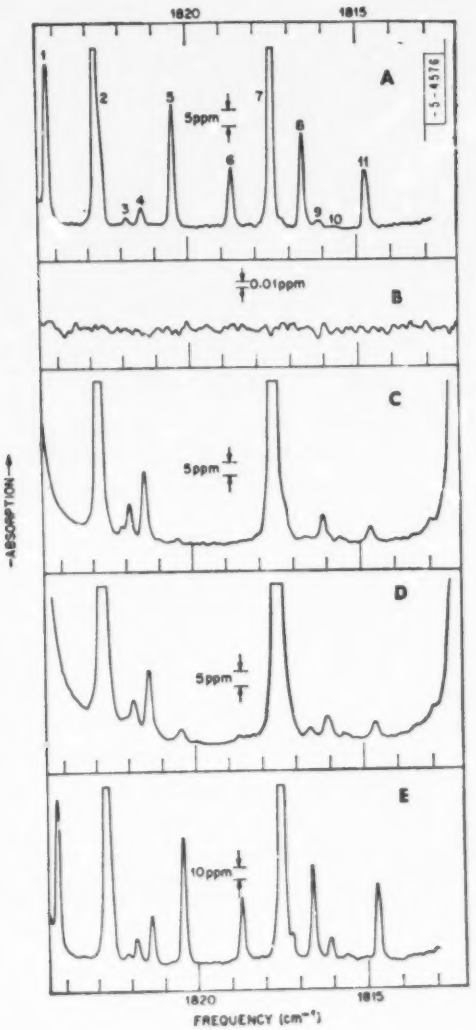

Fig. B-8. Detection of NO with an opto-acoustic detector using a tunable spin-flip Raman laser; (A) calibration scan of 20 ppm NO in N_2; (B) noise level with laser blocked; (C), (D), and (E) are scans for samples of laboratory atmosphere, ambient air near a busy highway, and exhaust gas from an automobile, respectively. All measurements were performed at approximately 300 Torr total pressure. Lines 1, 5, 6, 8, and 11 are due to NO – the rest are caused by water vapor. Reprinted with permission of the American Association for the Advancement of Science. After Kreuzer and Patel.[20]

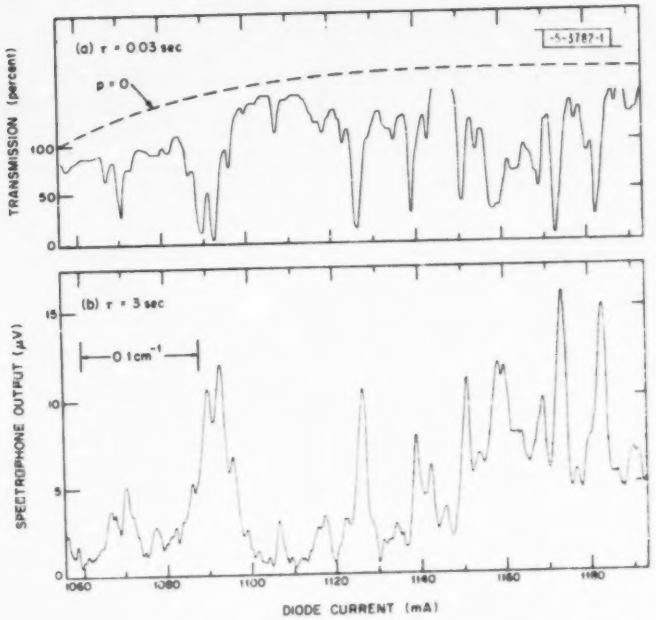

Fig. B-9. (a) Transmission scan for C_2H_4 in air using a $Pb_{1-x}Sn_xTe$ diode laser in the 10-μm region and a liquid-helium-cooled Ge:Cu detector. (b) Absorption sc[illegible] over the same spectral region using opto-acoustic (spectrophone) detection. [illegible] length is 10 cm, C_2H_4 pressure is 5 Torr, and air pressure is 15 Torr.

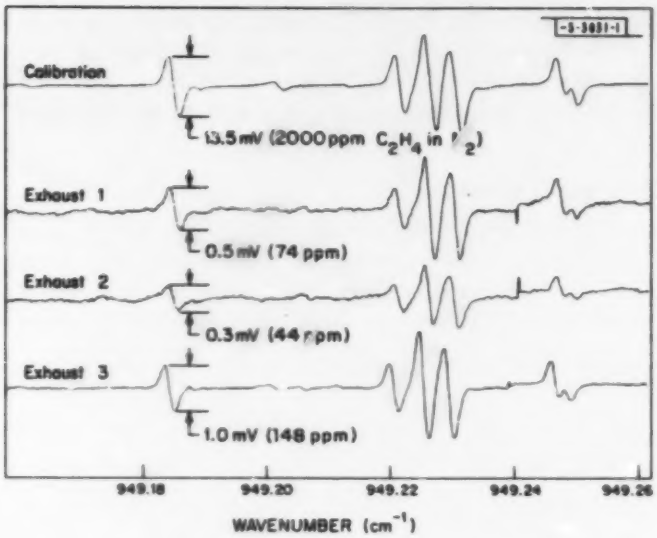

Fig. B-10. First-derivative spectra, taken with a $Pb_{0.88}Sn_{0.12}Te$ diode laser, of: (a) a calibration sample of 2000 ppm C_2H_4 in N_2 (top trace), and three automobile exhaust samples at different amplifier gain settings. Total pressure, 5 Torr; cell length, 30 cm.

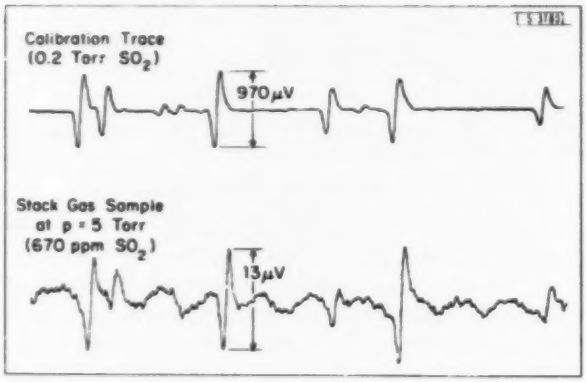

Fig. B-11 First-derivative spectra taken with a $Pb_{0.93}Sn_{0.07}Te$ diode laser, of 0.2 Torr SO_2 in the 8.7-μm region (upper trace), and a sample of stack gas reduced to 5 Torr pressure (lower trace). Cell length, 730 cm.

the derivative scan yields a value of 670 ppm for the concentration of SO_2 in the specimen. As with the automobile exhaust measurements, there appear to be no interferences from other gaseous components which are present. There is, however, a periodic background fluctuation caused by Fabry-Perot-type feedback from windows of the sample cell, which can be eliminated by proper design. It should be noted that these lines of SO_2 are not the strongest in the ν_1 band, and that the derivative signal would be 20 times larger if a more appropriate wavelength region were selected.[16]

3.3.2 In Situ Source Monitoring

A tunable-diode-laser system for across-the-stack monitoring of SO_2 is presently under construction at our Laboratory. The system, which is illustrated in Fig. B-12, yields an average value for the SO_2 concentration across the stack. This should be more representative than point-sampled values for predicting the total amount of SO_2 emitted into the environment. Preliminary

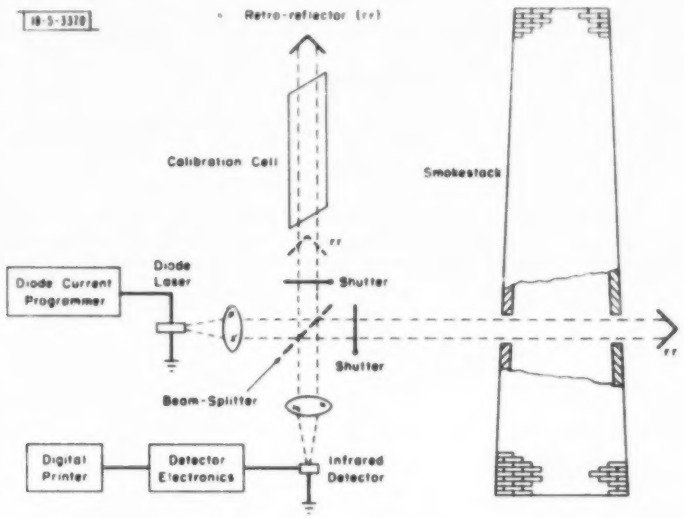

Fig. B-12. Diode laser system for across-the-track monitoring of pollutant gases in a smokestack.

work involved an extensive study of the 8.7-μm SO_2 band; the locations and strengths of over 200 lines were made by tunable-diode-laser spectroscopy, and compared with a theoretical model.[16] Other parameters, such as line-broadening coefficients, were also measured, and for SO_2 in the atmosphere the full linewidth at half-maximum intensity was found to be 0.3 cm^{-1}.

For the detection of pollutant gases in the atmosphere, where linewidths are relatively wide, pulsed-diode laser techniques can be used. By using pulses of current, rather than steady values, the cryogenic-cooling requirements are less stringent, and higher output laser powers can be achieved since larger injection currents are possible. The diode laser can still be tuned by a superimposed direct current. The power p_t received at the detector is related to the power p_o from the laser by the Beer-Lambert equation

$$p_t = p_o \exp[-\alpha'_c cL] \quad , \tag{3}$$

where the other symbols were defined earlier. With the aid of an integrate-and-hold circuit in conjunction with a logarithmic detector, as shown in the schematic of Fig. B-13, the recorded voltage is directly proportional to the pollutant concentration, c.

Application of this technique to on-line automobile exhaust monitoring was demonstrated by measurements made using a 1.15-meter-long optical path. Exhaust gas from an automobile was passed through a windowless tube through which the laser beam was also directed. Test results for a 1972 8-cylinder station wagon are shown in Fig. B-14 for two starting cycles: (a) a normal start where the accelerator pedal was not depressed; (b) a "rich" start. The measurement is essentially instantaneous, limited only by the rate of change of the C_2H_4 content in the exhaust. The C_2H_4 concentration of around 300 ppm during idle was confirmed by taking a sample and using the first-derivative technique at reduced pressure, described earlier.

3.3.3 Ambient-Air Monitoring

For ambient-air monitoring, where pollutant levels are usually much lower than they are near sources, sensitive detection can be achieved by long-path transmission or with the aid of multireflection cells. Although multireflection cell techniques are very susceptible to mirror contamination, tunable lasers can, by scanning alternately "on" and "off" an absorption line, eliminate most of the adverse effects caused by such variations in reflectivity. Of course, consideration must be given to the atmospheric "windows" when selecting appropriate wavelength regions.

At low pollutant concentrations, Eq. (3) can be approximated as follows:

$$p_t \simeq p_o(1 - \alpha'_c c_m L) \equiv p_o - \delta_p \quad , \tag{4}$$

where δ_p is the minimum detectable change in power. Solving for the minimum detectable pollutant concentration, c_m, we obtain

$$c_m = \frac{\delta_p}{p_o \alpha'_c L} \quad . \tag{5}$$

Under laboratory conditions, presently available infrared detectors can detect power variations of less than 10^{-11} W. In actual application, however, fluctuations in received laser power imposed by atmospheric turbulence, scattering, and equipment vibration may degrade this value. If we assume that the minimum detectable power δ_p is 10^{-9} W, that the laser power p_o is 100 μW, $\alpha'_c = 10^{-5}$ cm^{-1}/ppm, and a path length L of 500 meters, the minimum detectable concentration, c_m, is 0.02 ppb.

We have recently transmitted 10.6-μm radiation from a $Pb_{0.88}Sn_{0.12}Te$ diode laser over a 500-meter path, with a collection efficiency of 33 percent. The system used the electronic schematic shown in Fig. B-13. With the beam directed horizontally about 4.5 meters above a parking lot, an average increase of several ppm of C_2H_4 was detected during the late afternoon exodus of automobiles. The noise level for this test, with 2 μW of received laser power, was 120 ppb, caused primarily by relative vibrations in the optics.

4. CONCLUSION

There appear to be several important uses of tunable lasers for the monitoring of atmospheric pollutants, and some systems are already under construction. This field is very new,

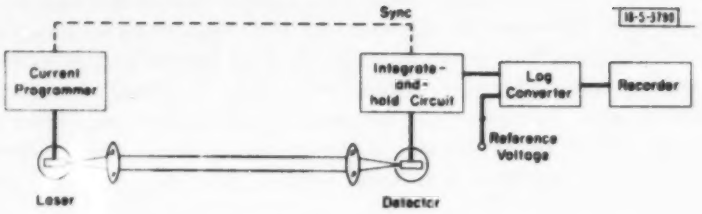

Fig. B-13. Operational schematic for general application of pulsed semiconductor diode lasers to the monitoring of atmospheric pollutants at emission sources or in the ambient air.

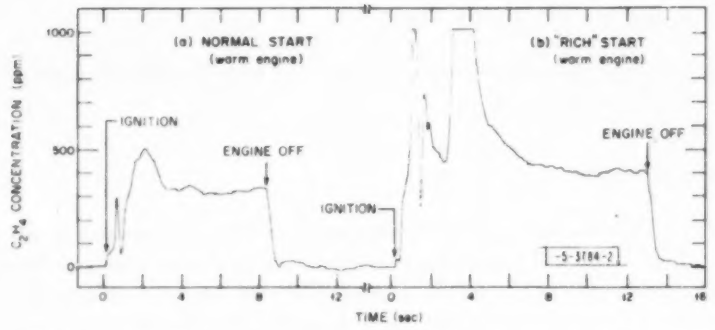

Fig. B-14. Results of an on-line emissions test for C_2H_4 in a 1972 station wagon, using a pulsed $Pb_{0.88}Sn_{0.12}Te$ diode laser operating at 10.57 μm. (a) represents a normal start of a warm engine, with ignition at time t = 0. For (b) the accelerator pedal was depressed during ignition, to produce a "rich" start, with significantly higher C_2H_4 emission.

less than two years old for the most part, and although requirements of low-temperature operation limit widespread use of some tunable lasers at present, improvements in both laser technology and advances in cryogenic cooler development should eventually eliminate this drawback for future monitoring applications.

ACKNOWLEDGMENTS

The author would like to thank H. A. Pike for permission to use pre-publication results of his spectrophone measurements and on-line automobile emissions data, R. S. Sinclair for designing the electronic circuitry for pulsed-laser monitoring, A. R. Calawa and T. C. Harman for developing the diode lasers, and K. W. Nill and F. A. Blum for providing their nitric oxide spectra. Appreciation is also expressed to J. O. Sample, T. E. Stack, and L. B. McCullough for very competent technical assistance.

REFERENCES FOR APPENDIX B

1. For a comprehensive review, including an extensive set of references to earlier work, see P. L. Hanst, "Advances in Environmental Science and Technology," Volume 2 (John Wiley & Sons, Inc., New York, 1971, edited by James N. Pitts, Jr. and Robert L. Metcalf), Chapter 4.
2. E. D. Hinkley and P. L. Kelley, Science 171 (1971) 635-639.
3. E. D. Hinkley and R. H. Kingston, Proc. Joint Conference on Sensing of Environmental Pollutants, Palo Alto, California, November 8-10, 1971.
4. H. Kildal and R. L. Byer, Proc. IEEE 59 (1971) 1644-1663.
5. I. Melngailis, IEEE Trans. on Geoscience Electronics GE-10 (1972) 7-17.
6. C. F. Dewey, Jr., and L. O. Hocker, Appl. Phys. Lett. 18 (1971) 58-60.
7. D. J. Bradley, Proc. Electro-Optical Systems Conference, Brighton, England, March, 1971; B. B. Snavely, Proc. IEEE 57 (1969) 1374-1390.
8. T. W. Hansch, I. S. Shahin, A. L. Schawlow, Phys. Rev. Lett. 27 (1971) 707-710.

8a. S. A. Tuccio and F. C. Strome, Jr., Appl. Optics 11 (1972) 64-73; A. Dienes, E. P. Ippen, and C. V. Shank, IEEE J. Quantum Electron. 8 (1972) 388.

9. S. E. Harris, Proc. IEEE 57 (1969) 2096-2113; R. G. Smith, "Optical Parametric Oscillators," in Laser Handbook (North-Holland Publishing Company, Amsterdam), edited by F. T. Arrechi and E. O. Shultz-DuBois (to be published).
10. J. Pinard and J. F. Young, Optics Comm. 4 (1972) 425-427.
11. R. L. Byer, VII International Quantum Electronics Conference, Montreal, Canada, May 8-11, 1972.
12. For a general review, with extensive references, see T. C. Harman, "The Physics of Semimetals and Narrow-Gap Semiconductors," proceedings of the Conference held in Dallas, Texas, 1970 (Pergamon Press, New York, edited by D. L. Carter and R. T. Bate); also, T. C. Harman, J. Phys. Chem. Solids Supplement 32 (1971) 363-382.
13. E. D. Hinkley, T. C. Harman, and C. Freed, Appl. Phys. Lett. 13 (1968) 49-51.
14. E. D. Hinkley, Appl. Phys. Lett. 16 (1970) 351-354.
15. K. W. Nill, F. A. Blum, A. R. Calawa, and T. C. Harman, Appl. Phys. Lett. 19 (1971) 79-82; , Chem. Phys. Lett. (to be published).
16. E. D. Hinkley, A. R. Calawa, P. L. Kelley, and S. A. Clough, J. Appl. Phys. 43, 3222 (1972).
17. C. K. N. Patel and E. D. Shaw, Phys. Rev. Lett. 24 (1970) 383-385; A. Mooradian, S. R. J. Brueck, and F. A. Blum, Appl. Phys. Lett. 17 (1970) 481-483.
18. C. K. N. Patel, Phys. Rev. Lett. 28 (1972) 649-652.
19. C. K. N. Patel, E. D. Shaw, and R. J. Kerl, Phys. Rev. Lett. 25 (1970) 8-11.
20. L. B. Kreuzer and C. K. N. Patel, Science 173 (1971) 45-47; R. A. Wood, R. B. Dennis, and J. W. Smith, Optics Comm. 4 (1972) 383-387; S. R. J. Brueck, E. J. Johnson, and A. Mooradian (private communication).
21. J. A. Rossi, S. R. Chinn, and A. Mooradian, Appl. Phys. Lett. 20 (1972) 84-86.

21a. I. Melngailis (private communication).

22. V. N. Bagratashvili, I. N. Knyazev, and V. S. Letokhov, Optics Comm. 4 (1971) 154-156; N. G. Basov, E. M. Belenov, V. A. Danilychev, and A. F. Suchov, Quantum Electron. (USSR) N3 (1971) 121-122; C. A. Fenstermacher, M. J. Nutter, W. T. Leland, and K. Boyer, Appl. Phys. Lett. 20 (1972) 56-60.
23. E. D. Hinkley and C. Freed, Phys. Rev. Lett. 23 (1969) 277-280.
24. R. J. Keyes and T. M. Quist, "Semiconductors and Semimetals" (Academic Press, New York, 1970, edited by R. K. Willardson and A. C. Beer), Chapter 8.
25. M. R. Bowman, A. J. Gibson, and M. C. W. Sandford, Nature 21 (1969) 456-457.
26. L. B. Kreuzer (private communication).